HEMISPHERICAL DISH MICROCONCENTRATORS FOR LIGHT-TRAPPING IN SILICON SOLAR CELLS

HEMISPHERICAL DISH MICROCONCENTRATORS FOR LIGHT-TRAPPING IN SILICON SOLAR CELLS

By

LETICIA MONTEIRO GONCALVES, B.Sc.

A THESIS SUBMITTED TO THE DEPARTMENT OF ENGINEERING PHYSICS AND THE SCHOOL OF GRADUATE STUDIES OF MCMASTER UNIVERSITY IN PARTIAL FULFILMENT OF THE REQUIREMENTS FOR THE DEGREE OF MASTER OF APPLIED SCIENCE

Master of Applied Science (2018) McMaster University
Engineering Physics Hamilton, Ontario, Canada

TITLE: Hemispherical Dish Microconcentrators for Light-Trapping in Silicon Solar Cells

AUTHOR: Leticia Monteiro Goncalves, B.Sc. (Nanotechnology)

SUPERVISOR: Dr. Rafael Kleiman

PAGES: viii, 66

ABSTRACT

To improve the performance of solar energy converters and its implementation as a more sustainable electricity source worldwide, researchers have been trying to increase the efficiency of photovoltaic devices while lowering their costs. Conversion efficiency of solar cells can be enhanced through light trapping structures and concentration of incoming light. Light trapping is usually realized by texturization of the solar cell's surfaces, while concentration is achieved by addition of external apparatus, such as reflectors.

A novel design for silicon solar cells is proposed in this thesis, which contains hemispherical dish microconcentrators for light trapping purposes. Through a process flow that includes maskless photolithography, thermal reflow, and metallization via sputtering, the microconcentrators were fabricated and demonstrated to have good concentration properties. Further studies need to be done for optimization of the hemispherical structures, as well as successfully perform the proposed upconverting photolithography for auto-aligned exposure of the photoresist at the microconcentrator's focus, thus allowing a complete solar cell to be created based on this design.

ACKNOWLEDGEMENTS

The author would like to thank Dr. Kleiman for the opportunity of conducting this research and his guidance and instructions. Extended thanks are directed to fellow members of Dr. Kleiman's research group for insights and helpful suggestions, particularly to Kevin Boyd, Abhi Rampal and Tim van Boxtel for the assistance in preparation of set-ups and execution of experiments, and Karl Petursson for reviewing this document's drafts. The author is also grateful for the training and advice provided by Doris Stevanovic and Dr. Shahram Tavakoli, as well as Dr. George Chiran for all the support and assistance offered in finding parts and organizing set-ups.

The author's gratitude is extended to Greice Monteiro for her encouragement and support that led the author to reach this achievement; and to Lucas Franceschinelli for the reassurance and support given, which was essential for this work to be completed. Finally, the author would like to show her appreciation for the help of friends and family who made the whole process much more enjoyable.

TABLE OF CONTENTS

Abstract iii
Acknowledgements iv
Table of Figures vii
1. Introduction 1
2. Background and Literature Review 4
2.1. Efficiency 4
2.2. Light Trapping 6
2.3. Concentrators 8
2.4. Hemispherical Structures for Light trapping 13
2.4.1. Nanostructures 13
2.4.2. Microlenses 15
2.4.3. Combination of Nanostructures and Microlenses 18
2.5. Conclusions 21
3. Design 22
3.1. Calculation 24
3.2. Simulation Modelling 30
4. Fabrication 31
4.1. Microconcentrators 32
4.1.1. Maskless Photolithography 33
4.1.2. Reflow 34
4.1.3. Sputtering 35
4.1.4. Recipe 36
4.2. Upconverting Photolithography 38
4.2.1. Upconverting Particles ..... **Error! Bookmark not defined.**
4.2.2. Upconverting Photolithography Set-up 40
4.2.3. Recipe 42
5. Characterization 43
5.1. Microconcentrators Properties 43

5.1.1. Geometrical Properties 43
5.1.2. Optical Properties 44
5.2. Upconverting Particles Emission 46
5.3. Photoresist Exposure 47
5.4. Upconverting Exposure 50
5.4.1. Laser Beam Profile 50
5.4.2. Upconverting Photolithography Using a Mask 51
6. Results 53
6.1. Geometrical Parameters 53
6.2. Focal Distance 55
6.3. Upconverting Exposure 57
7. Discussion 59
7.1. Upconverting Photolithography Process 59
7.2. Silicon Thickness 60
7.3. Microconcentrator Optimization 61
8. Conclusion 61
8.1. Future Work 62
References 63

TABLE OF FIGURES

Figure 2.1. SEM image of a pyramid texture silicon solar cell 8
Figure 2.2. Examples of CPV designs 11
Figure 2.3. 3D-printed concentrator arrays for external light trapping..... 12
Figure 2.4. Light-guide solar optic concentrator by Morgan Solar Inc. 12
Figure 2.5. Solar cell patterned with hemispherical nanoparticles……..14
Figure 2.6. Light trapping configuration using microlenses..... 16
Figure 2.7. Light trapping system with microlenses and a slab waveguide..... 18
Figure 2.8. Nanophotonic organic solar cell architecture. 20
Figure 3.1. Illustration of light trapping caused by a single microconcentrator.... 23
Figure 3.2. Structure of the proposed solar cell. 23
Figure 3.3. Illustration of pattern transferring process 24
Figure 3.4. Variables used in the calculation of the focal distance. 26
Figure 3.5. Initial thickness and width of hemispheres for given wafer thicknesses. 28
Figure 3.6. Variables describing the calculation of the focal distance with normal shift caused by new interface. 29
Figure 3.7. Zemax simulation result. 30
Figure 4.1. Process flow for microconcentrators fabrication 32
Figure 4.2. Design for exposing the cylinders using the direct writer 33
Figure 4.3. Optical microscope image of top left part of sample after direct writing exposure and development 34
Figure 4.4. Side view of photoresist structures before and after reflow process..34
Figure 4.5. Optical microscope image of top left part of sample after reflow 35
Figure 4.6. SEM image of sample after metallization 36
Figure 4.7. Absorption depth in Silicon 39
Figure 4.8. Upconverting photolithography process 40
Figure 4.9. Upconverting exposure experimental set up schematic 41
Figure 5.1. Profilometer measurement result..... 43

Figure 5.2. Optical characterization set up scheme. 44
Figure 5.3. Photo of the optical characterization set up. 44
Figure 5.4. Screenshot of the camera software 46
Figure 5.5. Emission spectrum of upconverting particles 47
Figure 5.6. Absorbance spectrum of S1800 series photoresist 48
Figure 5.7. Spectral radiance of monochromator output 49
Figure 5.8. Samples exposed by monochromator 50
Figure 5.9. Laser beam profile 51
Figure 5.10. Upconverting exposure using a mask 52
Figure 6.1. Hemisphere height measured at different values of diameter 54
Figure 6.2. Microlens height at different diameters 54
Figure 6.3. Focal distance of microconcentrators with different diameters 56
Figure 6.4. Modified upconverting photolithography process 58

1. INTRODUCTION

Solar energy systems are a current technology in our society. We can observe it in various implementations around us, from solar powered street lighting to rooftops panels and solar plants. It is evident that this technology has been attracting more interest over the years, especially after international agreements on lowering the world's carbon footprint. Direct solar energy is one of the key resources for large scale renewable energy harvesting. And for this reason, solar photovoltaics (PV) is the energy technology with the fastest growth in the world. In 2017, there was record global growth in solar PV, with newly installed capacity of approximately 402 GW (33% more than the previous year) [1] .

It is expected that, with proper incentives, solar PV could supply 30-50% of the global market share in electricity generation until 2050. This is a significant shift from the 1.9% representation projected by the end of 2017 [2], [3]. The key factors for sustaining the falling costs of solar PV are changes in markets, effective policies, new business models, and technological innovations. This is the reason why the research community is so interested in increasing energy conversion efficiency while maintaining affordable prices: that photovoltaics become widespread worldwide.

The great majority of solar cell production is currently based on crystalline silicon photovoltaics. Silicon is the most viable material for large-scale manufacture of solar cells, not only because it is earth abundant and non-toxic, but also due to its semiconductor properties. Its bandgap is close to the ideal value and it has good electrical properties, which makes it capable of reaching good efficiency even as a single junction device. Decades of experience in silicon processing from the microelectronics industry has made this semiconductor reach a technological maturity that has contributed to the continuous fall in prices of silicon wafers. For these reasons, it is likely that silicon will continue to be the dominant material used in solar cells.

The cost of silicon wafers has a big influence in the final price of a solar cell, since most of it comes from the value of silicon material and processing. Current solar cells in the market are made of silicon wafers with a few hundred microns of thickness. Although the ideal thickness for a silicon cell is about 100 μm, there is an increasing interest in thin film solar cells. With film thicknesses of a few microns and proper features for increasing light absorption, it is possible to considerably decrease the price of a silicon solar cell, while still having high efficiency.

Conversion efficiency is the ability to transform solar energy into electricity. Efficiency is an important characteristic of a solar cell, since it dictates how well the device performs. The maximum theoretical efficiency for silicon solar cells is about 30%. Although laboratory silicon solar cells are almost approaching this limit (the record is at 26.7%), there is still room to grow this percentage and to lower the costs of fabrication.

Different approaches can be considered for increasing the efficiency of a solar cell. It is known that solar concentrators and light trapping techniques are useful ways to obtain this effect. Generally, concentrators are composed by external apparatuses placed on photovoltaic modules to focus the sunlight on small solar cell surface areas. By doing so, the efficiency is enhanced since it is directly related to the photovoltage, which increases logarithmically with intensity. One example of a common solar concentrator is the design of telescopic parabolic dishes, which reflect the incident sunlight and concentrate it onto a solar cell placed on top of the dish.

Light trapping is usually achieved with texturization of the solar cell's surfaces. The purpose of this concept is to increase the optical path length of light inside the photovoltaic device, which can be achieved through refraction or reflection principles. By bending the light rays inside the solar cell, total internal reflection can occur, leading to the light being trapped within the device. This enhances light absorption by the solar cell, thus increasing its efficiency.

The goal of this thesis is to propose a new design for silicon solar cells that combines concentration and light trapping for efficiency improvement. The suggested device merges planar crystalline silicon solar cells and micrometer-sized reflective dish concentrators in a built-in wafer-level approach for increased light trapping. A combination such as the one explained here has never been seen before and its concept can be applied for different wafer thicknesses.

This novel design has hemispherical reflective dishes at the rear surface of a silicon solar cell that act as concave mirrors to reflect and concentrate incoming sunlight on the top surface, where the p-n junction should be located. With this architecture, light that would not be absorbed is trapped inside the solar cell and has its path length increased. The scope of this study was to create the design, fabricate and test these microconcentrators from an optics perspective.

Calculations based on key parameters that influence the microconcentrators' performance were conducted to find the best configuration. They are double checked through simulation modelling. These results were applied when fabricating the hemispherical structures. Fabrication followed a process flow that included maskless photolithography, thermal reflow, metallization via sputtering, and new type of photolithography process, called upconverting photolithography.

The upconverting photolithography was a solution found to allow an auto-aligned exposure to be performed using the microconcentrators created. It consists of mixing upconverting particles into a regular photoresist and exciting this mixture with a near-infrared laser. The upconverting particles absorb the longer wavelength radiation and emit in the ultraviolet range, exposing the nearby photoresist. The intention was to expose the photoresist coating on the top surface at the microconcentrators' focuses.

The process flow for fabricating the hemispherical concentrators proved to easily create structures with strong capacity of light concentration. Although the upconverting photolithography was demonstrated to be a viable technique, it was

not possible to accomplish an auto-aligned exposure throughout the course of this study. A few reasons are appointed for that and some suggestions are made for future attempts.

The design presented in this document is promising for application is silicon solar cells. Required optimizations are discussed in Section 7, which can be pursued as future work. Once the challenges presented by the auto-aligned photolithography are overcome, a complete solar cell can be fabricated and tested.

2. BACKGROUND AND LITERATURE REVIEW

The efficiency of a solar cell is the amount of sunlight that is converted into electricity. And there are different ways to improve it. One of them is by using light trapping features, which can stretch the time light stays inside the solar cell. Another method is the implementation of concentrators. They can increase the intensity of light entering the cell. Both concepts will be further discussed in section.

These methods inspired the new design for silicon solar cells proposed in this study, which combines light trapping and concentrators with the goal of enhancing a silicon solar cell's efficiency.

2.1. EFFICIENCY

Since the appearance of the first solar cell, people have wondered how well its performance could be in converting sunlight into electricity. Some relevant studies were done regarding the theoretical efficiency limit of a crystalline silicon single-junction solar cell under one sun. Different values have been concluded and that is due to assumptions and considerations of the authors in their calculations. For instance, the first prediction, done by Prince, stated that the maximum efficiency for a silicon-based cell would be of 21.7% [4]. About 6 years later, Shockley and Queisser introduced a new limit considering an energy gap of

1.1 eV, which would be 30% [5]. The work done by Tiedje and Yablonovitch, in 1984, set the limit for a crystalline silicon solar cell under AM1.5 to be 29.8% [6]. This result was later revised by Kerr et al., who got to 29.05% [7].

The value where it stands now is at 29.43% [8]. As it has been defined so far, this is the theoretical limit for a silicon solar cell's efficiency, which describes an ideal, perfect cell, of 110 μm thickness and made of undoped silicon. In practice, it is difficult to achieve this value. That is why Swanson has calculated, in 2005, that the practical limit for a realistic commercial cell considering it is built under the best conditions possible 10 years from then would be 26% [9]. This prediction was reassessed and reaffirmed in 2014 [10].

Although this percentage regards commercial cells, laboratory results have exceeded this amount. The latest efficiency record for a laboratory cell was reported to be 26.7% [11]. Most of the time, laboratory results are not scalable to commercial products due to processing restrictions, but in 2017, Kaneka Corporation announced they created a practical size cell of 26.6% efficiency that could be developed into a commercial product [12]. This means we are probably going to see more improvements of the solar cells available in the market soon. It is important to emphasize that as significant as approaching the theoretical limit is, keeping the prices low is a key factor to maintain the interest and growth of the solar energy sector.

There are several factors that influence conversion efficiency. They are: reference spectral irradiance from the sun; intrinsic characteristics of silicon; recombination, resistance, and optical losses. When it comes to the optical losses, the reflectance from both front and back surfaces must be considered. The front surface should let the incoming sunlight get in the cell, but it should not let it out. And the back surface needs to avoid transmission and reflect the light back, while the top surface must contain it. Light-trapping is a useful tool to achieve total internal reflection, so light is kept within the solar cell.

2.2. LIGHT TRAPPING

One way to improve the efficiency of a solar cell is by increasing its absorption of light at different wavelengths. When incident light is trapped inside a solar cell, the chances of absorption are increased, especially for longer wavelengths. With light trapping features, the optical path length is amplified as if the device was physically thicker. The effective absorption due to light trapping is dependent on the material's refractive index n. The theory, known as the Lambertian limit, expresses a maximum enhancement factor of $4n^2$ [13].

The indirect bandgap of crystalline silicon leads to a low light absorption in this material. Considering that, light trapping is very beneficial for this type of solar cells because of silicon's large refractive index, which can lead to an optical path length of ≈ 50 times the device thickness. Therefore, this technique has allowed thin film solar cells to have efficiency approaching the thicker versions. The concept of light trapping is implemented using the principles of rear surface reflection, angular incoupling of light and total internal reflection.

Rear surface reflection prevents photons to be lost due to transmission by reflecting them back into the solar cell. This way, the optical path length is at least doubled. If light enters the device at an angle and is reflected at the bottom, it can experience total internal reflection at the top surface and get trapped inside the solar cell. Structures used for rear surface reflection can be specular or diffuse. When specular, the angle which light is reflected is equal to its angle of incidence, in respect to the surface normal. Specular reflectors are usually made by dielectric or metallic materials. When diffuse, these structures reflect light in a variety of angles, not necessarily equal to the angle of incidence. Diffuse reflectors can be pigmented, as a layer of white paint, or textured, like metallic nanoparticles.

Angular incoupling of light makes incoming sunlight travel a longer distance to get to the bottom of the cell as the transmission through the cell occurs at non-normal angles. Larger angles of transmission can increase reflection at the rear

surface and decrease the front surface reflection, which leads to a total internal reflection effect. Angular incoupling of light can be achieved by texturization of the top surface, which will be commented on later.

Total internal reflection happens when light is travelling from a higher refractive index (n_2) medium to a lower n_1 medium. As a consequence of Snell's Law, the exit angle in the lower n medium is greater than the incident angle in respect to the surface normal. Therefore, there is a critical incident angle (θ_c) for which the exit angle approaches 90°:

$$\theta_c = sin^{-1}\left(\frac{n_1}{n_2}\right) \quad (1)$$

For incident angles greater than θ_c, total internal reflection occurs, and light is trapped inside the higher n_2 medium. For example, at an interface between silicon and air (n=1), if the refractive index of silicon at a given wavelength is 3.7, then the critical angle for total internal reflection would be 15.7°.

As mentioned previously, the most common way to achieve good light trapping is to introduce texturization to the surfaces. This changes the angle at which light travels in the device, which means that light will lose the memory of the external incident angle after bouncing a few times inside the cell. Texturization can be implemented on both top and bottom surfaces of the solar cell to increase total internal reflection. A popular example of textures used for this purpose is pyramids, with periodic or random distributions, that can refract incoming light [14]. Figure 2.1 shows an example of a pyramidal texturing for a silicon solar cell. But there are also other options found to be very efficient, such as zigzag on the bottom surface to increase a scattered reflection [15].

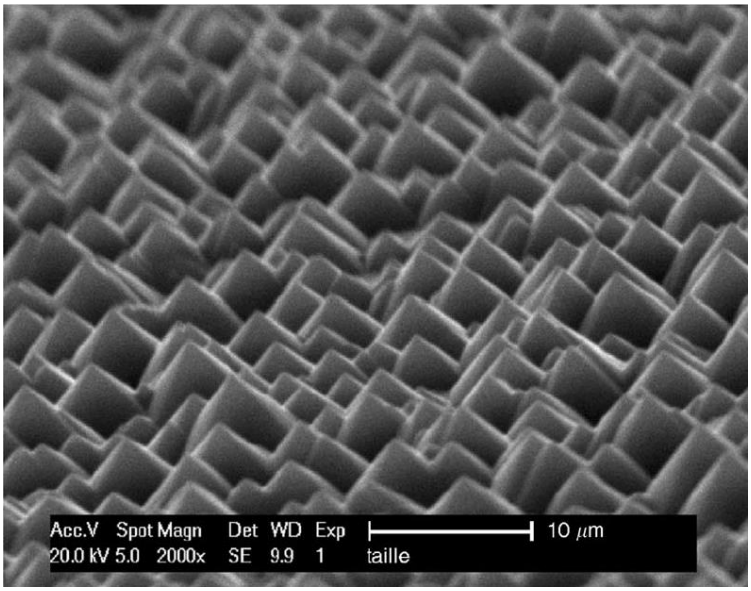

Figure 2.1. SEM image of a pyramid texture silicon solar cell. Reprinted from [16].

Recent studies have also demonstrated the application of photonic and plasmonic concepts into light trapping structures [17]. These features can increase the optical path length through scattering, concentration of light, or light coupling to guide it to the active layer of the solar cell. An additional aspect of photonic techniques is the possibility of bandgap engineering to change absorption and extraction of photons in the solar cell. Some examples of structures used for this purpose are nanocrystals and nanowires [18], 1D and 2D lattices [19], and optical filters [20].

2.3. CONCENTRATORS

Concentrator photovoltaics (CPV) uses optical elements, such as lenses and curved mirrors, as an additional strategy to enhance the efficiency of solar energy systems. These structures focus or guide the incident sunlight onto a small high efficiency solar cell, increasing the number of suns and, consequently, the intensity of the light beam hitting the cell. Under normal incidence, the maximum concentration possible on earth's surface is of 46,200 suns [21].

Since the solar cell is the most expensive part of a solar energy system, concentrators have emerged as an attempt to lower the cost related to flat-plate photovoltaics since a smaller area can be occupied by the solar cell under concentration. And because of the amplified power coming to the device, CPV has a higher efficiency potential than one-sun photovoltaics. For silicon solar cells under concentration the efficiency can be around 36-37%, which exceeds the Shockley-Queisser limit [22].

There are different types of systems and they are classified according to their concentration factor. If sunlight is amplified by a factor between 2 and 100, then the system is considered of low concentration (LCPV). In the cases where the factor is from 300 to 1000 times, the system is said to be of high concentration (HCPV). High concentration systems are usually coupled with high efficiency multi-junction solar cells, and usually require large areas for their implementation.

Because only direct sunlight can be effectively concentrated, these CPV structures need mechanical tracking to maintain the system aligned with the sun. Amplifying the intensity of incoming light with concentrators can make solar cells reach an elevated temperature, which can be detrimental to its efficiency. That is why cooling systems of some sort are needed to ensure high efficiency. In the case of low concentration systems, silicon solar cells are the common choice due to economic reasons. And because these systems have a low heat flux, active cooling is not required. Cost-effectiveness of CPV systems depend on the total cost of the optics, assembly and mechanical tracking, which cannot exceed the amount saved from using small area solar cells.

The main approaches used in concentrator technologies are refractive, reflective, and luminescent. Figure 2.2 shows examples of each kind. Solar concentrator system can combine more than one of these principles in their design.

Refractive concentrators rely on refraction to bend light rays and focus sunlight on solar cells. The most common example of refractive concentrators are Fresnel lenses (Figure 2.2a), which are composed by various sections with different angles to allow a large aperture and short focal length. Fresnel lenses are usually made from plastics such as PMMA or PDMS adhered to a glass structure. They can achieve medium to high concentration ratios.

Reflective concentrators are based on mirrors which reflect sunlight towards the solar cell. There is a variety of designs using reflective concentrators, such as parabolic dishes, compound parabolic concentrator and reflectors (flat, v-trough, linear…). The main materials used are silvered glass, polished metals or aluminized plastics. Reflective systems have concentration ratios ranging from low to high, depending on their design. With secondary optics, higher concentrations and a more homogeneous light flux can be obtained. Parabolic dishes are a good example of high concentration reflective systems. In this design, incoming parallel light is collected by the first parabolic mirror and reflected, through a focal point, onto a second mirror, which then reflects the light rays onto the solar cell located in the middle of the first mirror (Figure 2.2b).

Luminescent concentrators are composed by transparent plastic body in which luminescent species (organic dye molecules or quantum dots) are dispersed (Figure 2.2c). These particles absorb incident light and emit photons isotropically at an energy ideally just above the band gap of the attached solar cells, with high quantum efficiency. Internal reflection guarantees that part of the emitted light is transported through the plastic body and collected by the solar cells placed on its sides. Luminescent concentrators can absorb both direct and diffuse light with a concentration factor of 5-10, with no need of tracking apparatus.

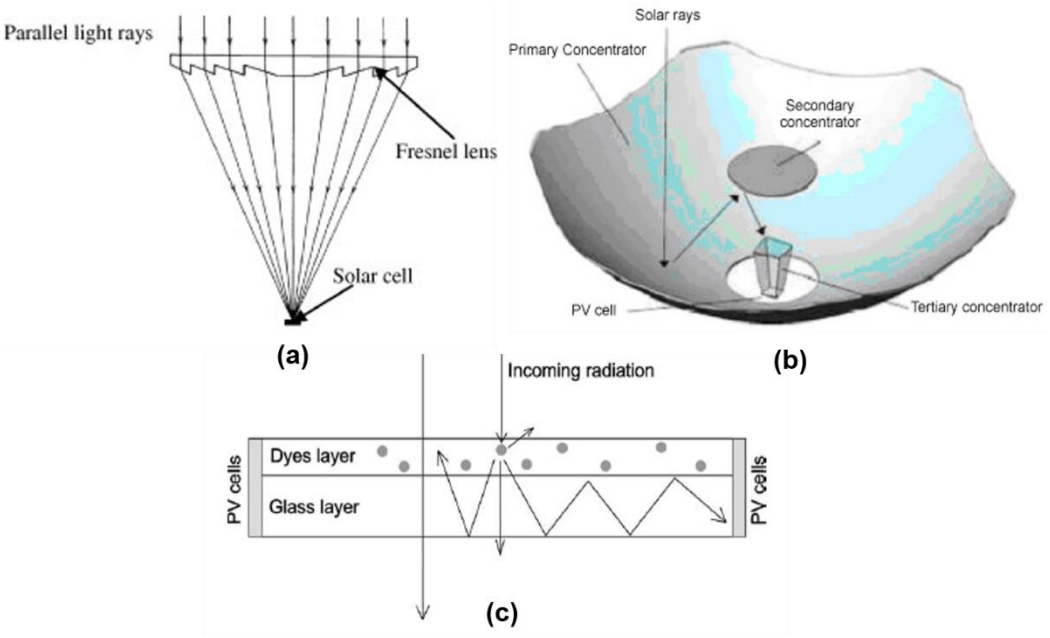

Figure 2.2. Examples of CPV designs with (a) Fresnel lens [23], (b) parabolic dish, and (c) luminescent concepts [24].

There are examples in the literature and in the market where concentrators are being used as external light trapping structures. One of this designs suggest the use of 3D-printed concentrators for thin film solar cells [25]. In this study, parabolic concentrators focus sunlight through a small aperture and a spacer allows photons that are reflected by the solar cell to be redirected back towards it due to the reflective coating of the cage (Figure 2.3). This system increases the probability of absorbance by the solar cell thus leading to a higher power conversion efficiency. Another interesting example of a concentrator applied in a light trapping concept is the light-guide solar panel created by Morgan Solar [26]. Their system consists of an ultra-thin dielectric optical structure that traps sunlight internally and redirects it onto a small high-efficiency solar cell in the centre of the assembly (Figure 2.4). This allows the system to save space compared to regular concentrators that need extra room due to the focal depth.

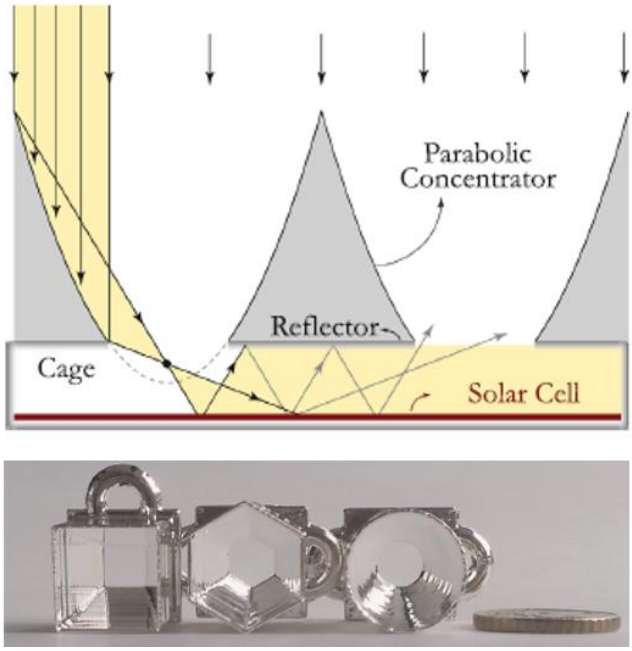

Figure 2.3. 3D-printed concentrator arrays for external light trapping. Top: schematic with ray tracing showing light trapping. Bottom: designs tested [25].

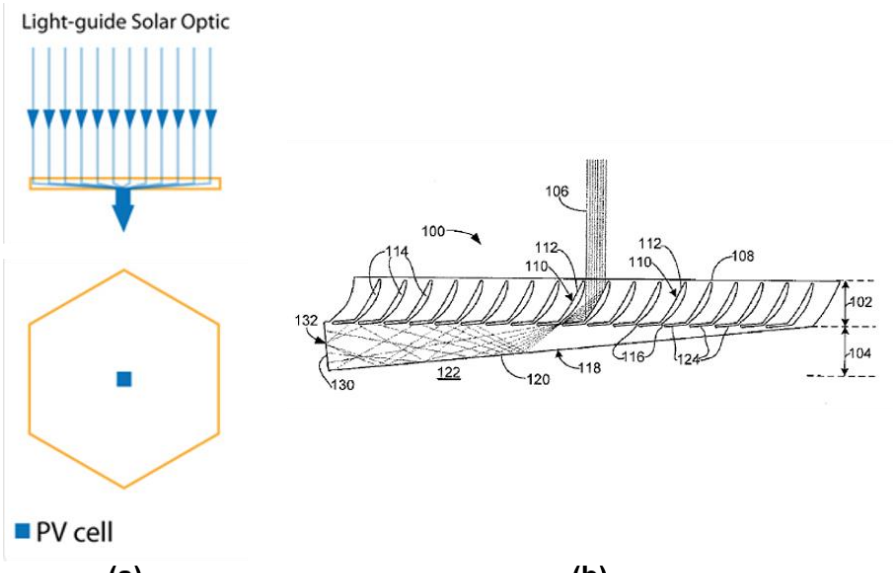

Figure 2.4. Light-guide solar optic concentrator by Morgan Solar Inc. (a) Schematic of system [27]. (b) Ray tracing showing light trapping features [26].

2.4. HEMISPHERICAL STRUCTURES FOR LIGHT TRAPPING

Although the most common pattern used for light trapping textures are pyramids, it is possible to find different shapes applied for this purpose in the literature. Hemispherical assemblies that can appear in forms of nanoparticles, microlenses, or a combination of both, are a good example. Below some studies discussing these hemispherical structures are presented.

2.4.1. NANOSTRUCTURES

Ferry *et al.* designed and fabricated hemispherical nanostructures to act as a plasmonic light trapping system in ultrathin film a-Si:H solar cells of less than 100 nm thickness, using a wafer-scale soft imprint lithography combined with deposition techniques [28]. They studied nanodomes of varying diameters of 200, 290 and 310 nm distributed in 13 periodic and random array patterns. These metal nanostructures where embedded into the back contact the solar cell, transferring the hemispherical shape through its subsequent coating layers. Figure 2.5 shows the three-dimensional solar cell fabricated.

Their goal was to increase the path length and short current density by trapping light into in-plane waveguide modes of the semiconductor layers near the surface. They also determined the influence of spatial correlations and surface topography of scattering nanostructure arrays in the photocurrent spectrum for the high efficiency a-Si:H solar cells created, which contained integrated plasmonic and Mie scattering nanostructures.

The challenge faced by the group was to understand the relation between spatial frequencies and curvature of the nanoscatterers in the three-dimensional structure for a broadband, isotropic angular response. From this analysis, they could design the ideal random pattern and create the localized and propagating modes resulting from the plasmonic back reflectors and the surface Mie scatterers. Through this study, they could validate their simulation results with a

sample of ultrathin solar cell with broadband photocurrent enhancement in the blue and the red portions of the spectrum.

They believe that instead of having a one-step deposition processing, if the pattern construction could be decoupled at the two interfaces of interest, higher efficiencies would be achieved. And this design might then be applicable to non-conformal semiconductor depositions. They also state that the principles discussed are theoretically valid for other solar cell systems made of different materials than the hydrogenated amorphous silicon used.

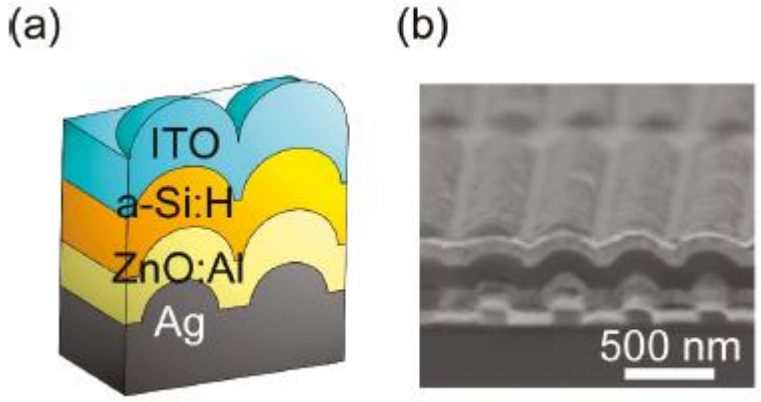

Figure 2.5. Solar cell patterned with hemispherical nanoparticles. (a) Scheme. (b) SEM cross section. Reprinted from [28].

A solar cell with a similar purpose was suggested by Zhang *et al.*, where a thin-film silicon solar cell with dual photonic crystals design was proposed [29]. In their paper, they investigate the influence of shapes and heights of top and bottom arrays of conformal and non-conformal nanocones and propose a method for determining the shape of these structures. After systematic optimizations through simulations, they analyze the separate contributions of each layer to the light harvesting and get to the conclusion that the top nanocones have a greater impact in light harvesting.

They also affirm that the height of both top and bottom arrays strongly impacts the performance of the thin-film cell. The results obtained, show that

when their heights (from top and bottom nanocones) are not the same, a better light trapping is achieved compared to the conformal system. For conformal nanocones, a parabolic shape is ideal for both top and bottom arrays. But for a better result, the optimal height of top and bottom nanocones differs between each array, as well as their shapes. For this non-conformal system, the top nanocones should have a parabolic shape, while the bottom ones should be needle-shaped.

2.4.2. MICROLENSES

Different configurations have been studied where plano-convex microlenses are employed in light trapping systems. Some relevant examples are presented below.

In the study by Tvingstedt *et al.*, arrays of semi spherical and semi cylindrical microlenses were implemented in a light trapping configuration featuring micro apertures formed in a reflective surface that faced thin film organic solar cells [30]. In their design, incident sunlight is concentrated by the microlenses and focused into self-aligned apertures towards the solar cells (Figure 2.6). Photons that are reflected by the solar cells back to the top surface would then hit the mirror layer between the apertures and have another chance to be absorbed by the photovoltaic device. Multiple bounces can happen between the surface of the cell and the back of the trap system. This way, reflected photons are recycled, enhancing absorption rate of solar cells with limited photon absorption and increasing their photocurrent up to 25%, and consequently, their efficiency.

The fabrication of this light trapping structure comprises patterning a quartz substrate with an array of concave lenses through a photolithography followed by an etch processing, which is then used to imprint the pattern into a malleable optical resin on a glass or transparent plastic substrate. The microlenses created

are used to perform a self-aligned exposure to generate the apertures in the metal layer deposited on the other side of the substrate.

The group claimed that a limitation of this system is its sensitive angle dependence due to the possibility of incident sunlight coming at an angle out of a perpendicular alignment. This could cause light to not be focused into the apertures, thus not illuminating the solar cell. The issue would be more critical with the 2D array containing hemispherical micro lenses than with the 1D hemicylindrical version, where alignment only in the plane parallel to the axis of the lenses is enough. They also conclude that the proposed light trapping system can be useful for other types of solar cells that may reflect part of the sunlight rather than absorb it, and not only for low cost organic photovoltaics.

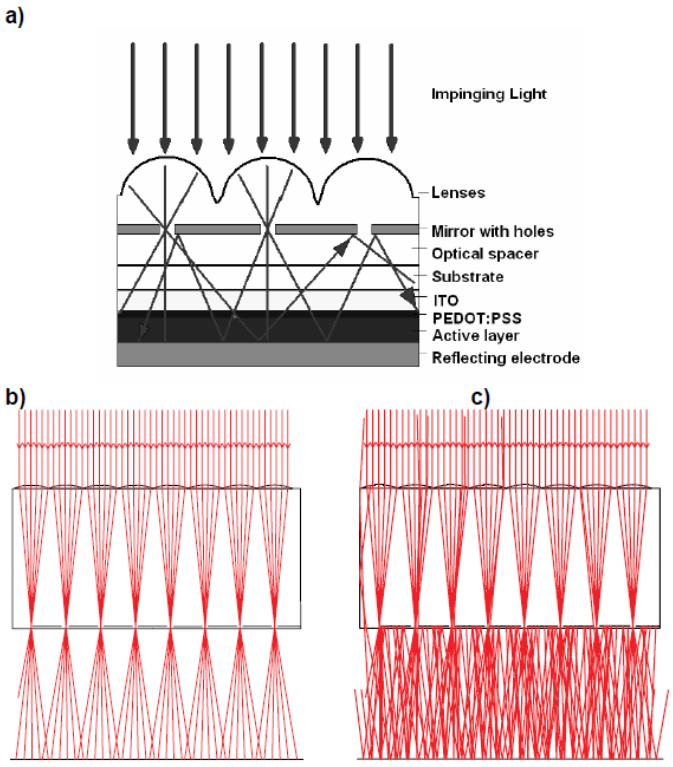

Figure 2.6. Light trapping configuration using microlenses. (a) Structure; (b) ray tracing simulation with 100% absorbing solar cell; (b) ray tracing with 100% reflecting solar cell. Reprinted from [30].

Karp *et al.* conducted another study using microlenses associated with light trapping system that is in some ways similar to the one presented by Tvingstedt's group, but with a concept more focused for use as concentrators. Instead of a photon recycling system, Karp *et al.* propose a design where a multimode slab waveguide is used as secondary optics of a micro-concentrator system, which collects and homogenizes sunlight focused by a lens array and transport the concentrated and trapped light onto a single high efficiency solar cell (Figure 2.7a) [31]. Their goal was to create an alternative thin, flat geometry for moderate concentration that could be manufactured by a low-cost roll processing and mounted for two-axis tracking, while avoiding the use of multiple secondary optics and their associated costs.

The system's operation is based on the microlenses concentrating incident sunlight into a planar waveguide slab with self-aligned apertures and coupling facets localized where each lens focus is. The sunlight collected by the apertures input is transported through the waveguide to a photovoltaic cell at the edge of the waveguide. The couplers are reflective prisms placed on the backside of the slab that have the role of fold mirrors, deflecting sunlight at angles that exceed the critical angle for total internal reflection inside the waveguide.

The prototype created to test their proposal used a commercial hexagonal lens array to perform a self-aligned exposure. The lens array was placed on the opposite side of a glass slab coated with a SU-8 photoresist layer previously molded with a prism array pattern. UV illumination was shone through the lens array, exposing the photoresist at each focal plane, and leaving the couplers there after development. With this method, the group obtained a 37.5x prototype concentrator with 32.4% optical efficiency.

There are some challenges appointed by the authors. One of them is to obtain an optimized coupler size since it defines the angular acceptance of the concentrator. If the coupling regions are oversized, the acceptance angle is broadened, which allows the focus to remain incident on the coupler even with a

little misalignment with the sun. On the other hand, if the area covered by the couplers is too large, the probability of decoupling increases, which might decrease optical efficiency. Other design factors that must be optimized due to their great influence on the system's performance are: the lens dimensions, waveguide numerical aperture and tilt angle of the coupling facets.

The authors expect that systems with optical efficiency above 80% and 300x concentration can be obtained when introducing custom lens arrays with better performance than the commercially available ones used in the prototype. They did present optimized performance and design variations in a later study [32].

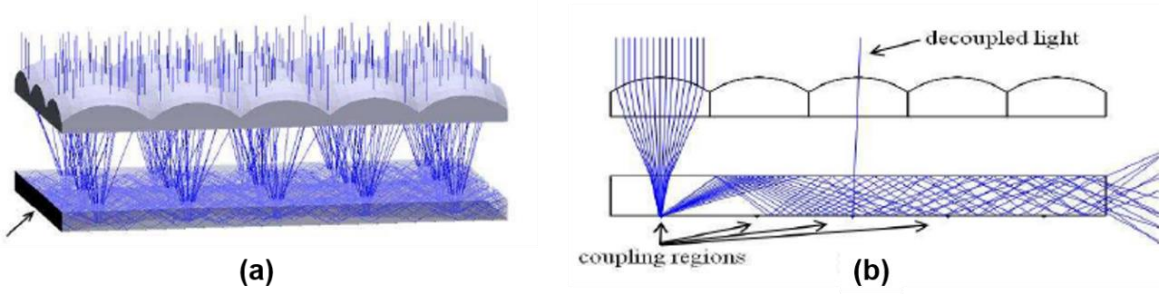

Figure 2.7. Light trapping system with microlenses and a slab waveguide. (a) Sunlight is concentrated by the microlenses through apertures in the optical slab which guides it to a single cell placed at the edge of the slab (indicated by the arrow). (b) Coupling regions are present at the bottom surface of the waveguide to increase optical efficiency. Reproduced from [31].

2.4.3. Combination of Nanostructures and Microlenses

Peer and Biswas combined microlenses and photonic-plasmonic crystals in a light trapping system to increase broadband light absorption of an organic solar cell [33]. In their design, polymer microlenses located on top of a glass slab focus incoming sunlight onto a periodic metal nanostructured array on the bottom of the solar cell, which diffracts the light (Figure 2.8). This coupling creates waveguiding and surface plasmon modes that increase long wavelength absorption by the solar cell due to light scattering and electric field enhancement in the active layer.

With the improved absorption, the proposed solar cell approaches the Lambertian limit for its kind.

The authors planned the design considering easy fabrication methods. The microlens array can be manufactured by lithography interference and placed on top of the glass substrate without interfering with the properties of the organic solar cell, which is situated in the opposite side of the substrate. The nanostructured conical pillars can be created on the organic layer by nanoimprinting, followed by a metal cathode deposition step. The pitch of both structures (microlens and nanocones) is a critical factor for light management and diffraction, whereas the height does not influence the performance that much. An ideal solar cell with this architecture must have microlenses and nanocones with the same pitch, and it was found that a period of 500 nm for both arrays results in an absorption increase of 49% and a photocurrent enhancement of 58% relative to a flat version of this solar cell. Unavoidable misalignment between the microlenses and the nanocone array positions are likely to happen, but if it does, the enhancement factor would only be reduced by about 1%. This indicates that the system is not sensitive to common fabrication constraints.

When analyzing the roles of the microlenses and the nanocones in the maximal enhancement in absorption and photocurrent of an optimized architecture, the group observed that the high increase in absorption is mainly caused by the patterned metal cathode. That is because it is responsible for diffracting light and generating surface plasmons, which enhances the field intensity at the organic-metal interface. On the other hand, the microlenses contribute by further increasing the plasmonic effects through focusing the light within the organic absorber layer. When comparing the enhancement in the solar cell performance caused by each feature, it was observed that with only the microlenses (on top of a flat internal interface) an improvement of ~13% in both absorption and photocurrent would be obtained. Whereas for only the nanostructures in the organic-cathode interface (no microlenses), the increase

would be of 40% in absorption and 50% in photocurrent. In the case of coupling both features, the ideal solar cell would have an increase in absorption of ~49% and ~58% in photocurrent.

When considering realistic metal and ITO in their simulation, using a real space methodology, the authors obtained a result where the photocurrent would be increase by 38%, while the weighted absorption would increase by 36%. This difference compared to the ideal scenario is a consequence of parasitic losses that happens mainly in the metal cathode. The authors then conclude that the proposed design would be an experimentally realizable architecture with a potential to achieve more than 12% efficiency for single junction organic solar cells.

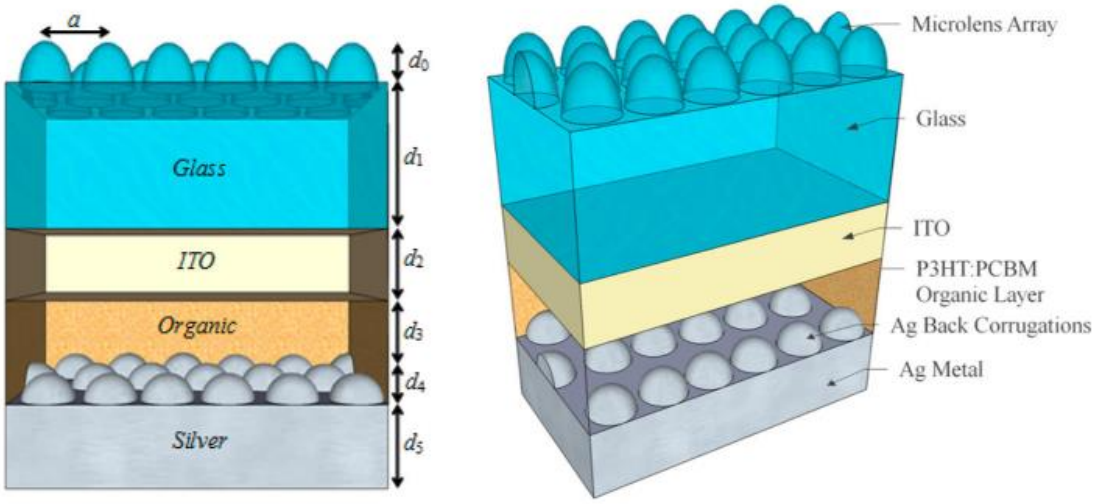

Figure 2.8. Nanophotonic organic solar cell architecture (not to scale). Reprinted from [33].

The observation that microlenses by themselves do not contribute much to the enhancement factor in a solar cell's photocurrent agrees with results obtained in the study by Tseng *et al.* [34]. In their research, they determined the effect of a cylindrical microlens array acting as a concentrator to enhance photovoltaic current in silicon solar cells. The authors compared systems consisting of a plastic solar concentrating optical film with and without horizontal cylinder

microlenses attached on the surface of a silicon solar cell. From experimental results, they observed that the optimized patterned film increases the gain of photovoltaic power in ~3.3% relative to a system with no microlenses. That is because these microlenses efficiently refract incoming sunlight, reducing the chances of reflection and increasing the absorption in the solar cell, with the advantage of not requiring a solar tracking mechanism.

2.5. CONCLUSIONS

In terms of strategy using hemispherical shapes in solar cells, microlens arrays are the main resource for obtaining concentrating features with the same magnitude of the photovoltaic device, and they can be implemented in any type of solar cell. When it comes to light trapping goals, plasmonic-photonic rounded nanostructures are a common tool used in thin films and organic solar cells. These nanostructures can also be combined with microlens arrays to further increase the efficiency of the system.

Fabrication of both structures generally involves some type of photolithography, which might be combined with molding techniques, and metal deposition, in case of reflective (and conductive) surfaces. The geometric characteristics of the hemispheres and the array pitch have great influence on how these structures enhance absorption and photocurrent in the solar cell, which determines its efficiency. This relation and optimization can be checked through different methods of simulation.

Although plasmonics and photonics structures play a more effective role in enhancing photovoltaic properties than microlenses, their performance is very dependent on tuning frequencies and obtaining the appropriate curvature of the nanoparticles, so an ideal isotropic spatial distribution of the trapped light occurs. On the other hand, the effect of adding microlenses in the system is easily achievable. Microlens arrays are often presented as an external apparatus placed above the solar cell, while nanoparticles are usually embedded in the

photovoltaic device at its bottom surface. Considering that, adding microlenses to the photovoltaic system generally does not influence the solar cell design and fabrication, since it can be created separately and only attached to the solar cell. In the case of nanoparticles, they become part of the solar cell design, since they have to be implanted in it (usually in the interface between the active layer and the metal back contact).

From the trends found in literature, it could be observed that studies usually present designs where microlenses are used as concentrators and hemispherical shapes placed at the bottom of the cell act as convex reflectors. Concave reflective structures located at the bottom surface of a solar cell were not found to be considered as a concentrator or light trapping strategy so far.

3. DESIGN

In this thesis, a novel design for silicon solar cells is proposed. It combines the concepts discussed in Section 2 by using microconcentrators as light trapping structures in a way that has not been reported so far by other studies. In this proposal, hemispherical reflective dishes are formed at the bottom of a silicon solar cell to act as concave mirrors. This way, when sunlight goes through the solar cell, the light that was not absorbed will be reflected back and concentrated on the top surface where the p-n junction will be located, thus increasing the chances of getting absorbed. The idea is to trap light that was not absorbed at first and have its path length increased (Figure 3.1).

An additional motivation behind this design is to avoid chromatic aberrations by placing the reflectors at the bottom of the silicon wafer. For this reason, it is also important to ensure incoming light rays are as parallel to the top surface normal as possible. Therefore, it is also critical to have solar tracking added to the system when implementing this design, to ensure the solar cell is always facing direct sunlight.

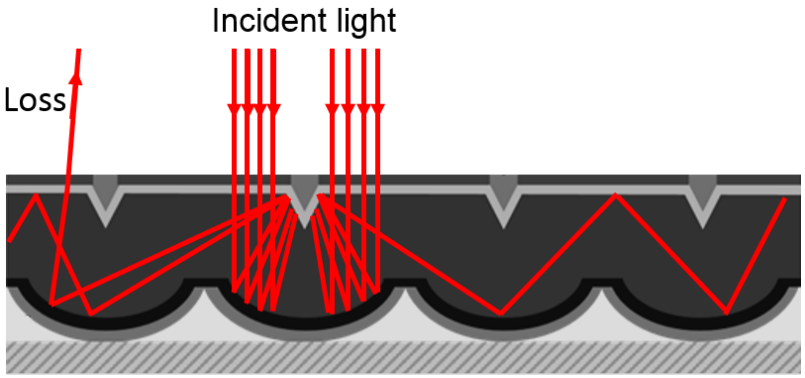

Figure 3.1. Illustration of light trapping caused by a single microconcentrator.

The purpose of this study was to create the design, fabricate the microconcentrators and test them from an optics perspective. Proving these microconcentrators could improve light trapping in the silicon wafer, allows future application in a silicon-based solar cell to be pursued. However, a complete cell was not fabricated during this project. Nevertheless, Figure 3.2 shows how the proposed design could be used to manufacture a complete solar cell structure.

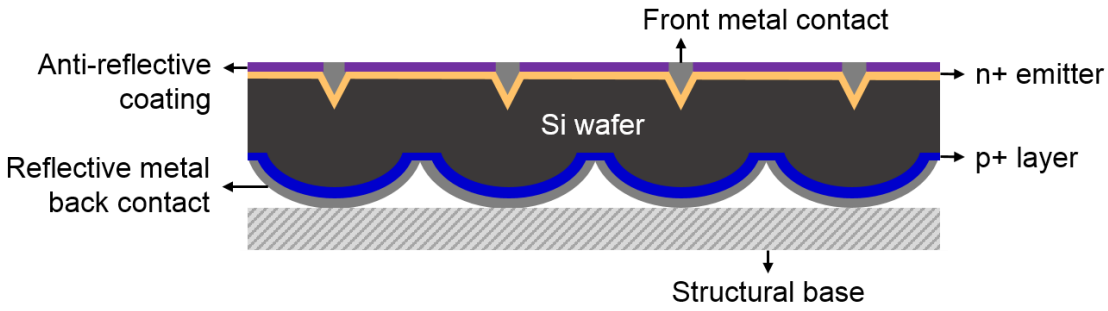

Figure 3.2. Structure of the proposed solar cell.

It is important to highlight that ideally the microconcentrators would be made of the same material as the solar cell, in this case, silicon (as seen in Figures 3.1 and 3.2). This feature is important to avoid chromatic aberrations that could be detrimental to the device's performance. But to produce these hemispherical structures and test them in a timely fashion for this project, the microconcentrators were created in a photoresist layer and tested that way. In

order to transfer these hemispherical structures from photoresist to silicon later, an additional step of reactive ion etching (RIE) would have to be added in the fabrication process flow described in Section 4. The RIE process allows one to transfer a pattern from one material to the other through a dry etching method that, when set to a specific gas ratio, can remove the photoresist coating the wafer, while leaving the silicon to have the same pattern presented previously by the photoresist, as seen in Figure 3.3.

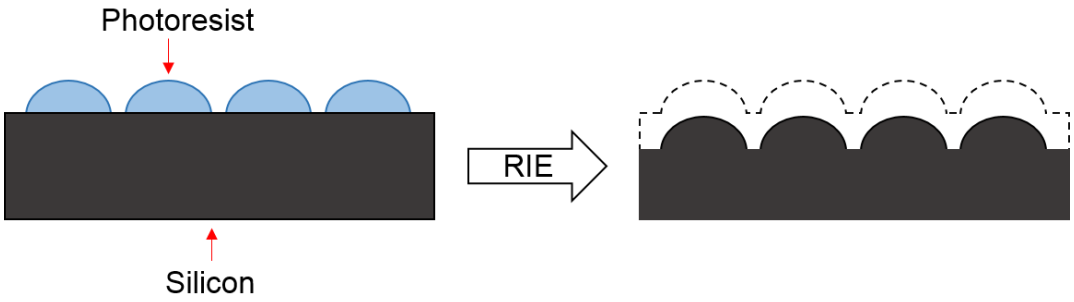

Figure 3.3. Illustration of pattern transferring process from photoresist to silicon.

The following subsections describe in more details the microconcentrator design and which parameters are important for increasing the performance of these structures.

3.1. CALCULATION

The performance of the proposed design depends on the microconcentrator's ability to focus light on the top surface of the silicon wafer, so the intensity of the concentrated light will be stronger there. For this reason, it is important to have control of the parameters that influence where the focus is.

Some calculations were done to find the best configuration of the microconcentrators. They were based in key parameters that influence where the focal distance is, which are: the wafer thickness, the concentrator's height, its width, and the initial thickness of the photoresist (before exposure and the emergence of the hemispherical shape that will become the microconcentrators).

These calculations were done assuming an ideal scenario, where the concave mirror is perfectly spherical.

The wafer thickness is a fixed value that only depends on the choice of wafer used as a substrate. It must be taken into consideration because it sets where the concentrator's focus must be, since the focus needs to coincide with the top surface. It is important to note that the wafer thickness also plays a significant role in the final device's performance as a solar cell since thicker wafers would make it more expensive, while thinner wafers would have a weaker absorption.

The initial thickness of the photoresist is a fixed value that had to be chosen, so we could have a starting point for defining other variables which were dependent on it. Based on the characteristics of the thick positive photoresist available, the recipe developed was set to result in a 25 µm-thick coating. Although, this number might vary due to experimental conditions. Therefore, the real thickness value obtained in the experiment was used for the calculations on a case by case basis.

The concentrator's height and diameter compose the radius of curvature, R, which divided by two, can determine the focal length, f, of a spherical concave mirror (Equation (2)).

$$f = \frac{R}{2} \tag{2}$$

The radius of curvature can be calculated using Equation (3):

$$R = \frac{h}{2} + \frac{w^2}{8 \times h} \tag{3}$$

where h is the hemisphere's height, and w is the hemisphere's width (also referred to as diameter).

The photoresist initial thickness, t, relates to the final height and the concentrator's diameter according to equation (4), which assumes an ideal spherical surface and that the volume is conserved when the photoresist pattern goes from a cylinder to a hemisphere [35].

$$t = \frac{h}{6}\left(3 + \frac{h^2}{r^2}\right) \tag{4}$$

where

$$r = \frac{w}{2} \tag{5}$$

So, to obtain a concave mirror with the ideal focal length, the most suitable diameter and height need to be determined, based on the set initial thickness of the photoresist, in order to get to R.

Because the refractive indices of the photoresist and the silicon wafer are different, there is a shift of the focal length inside the silicon slab that needs to be considered when doing the calculation. Therefore, by Snell's Law and small angle approximation, the normal shift of the focal distance due to the change in refractive index can be calculated using Equation (6):

$$\frac{n_1}{S'} + \frac{n_2}{S} = \frac{n_2 + n_1}{R_{int}} \tag{6}$$

where n_1 is the refractive index of silicon (3.57); n_2 is the refractive index of the photoresist AZ 40XT-11D (1.57 at 980 nm); S is the focal distance from the interface between silicon and the photoresist, S' is the focal distance from the interface due to the shift, and R_{int} is the radius of curvature of this interface. The variables are illustrated in Figure 3.4.

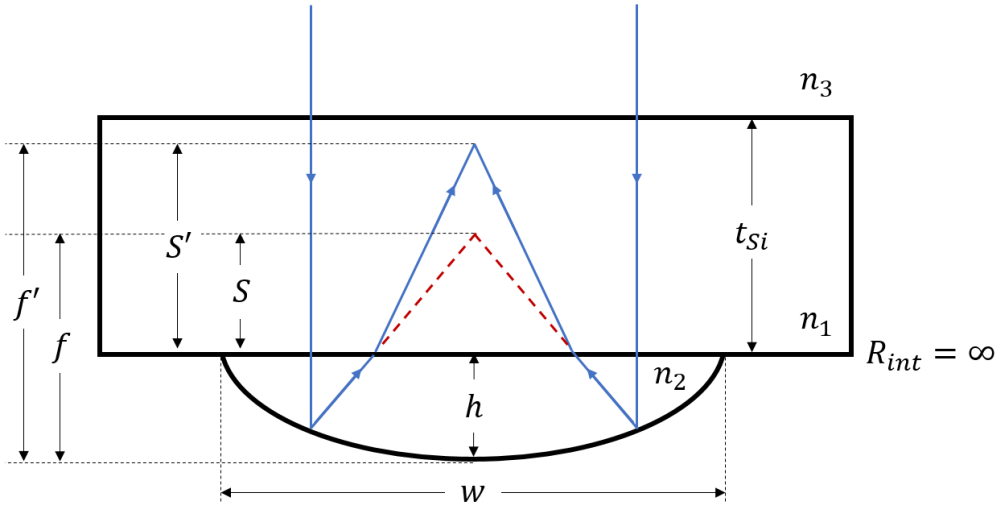

Figure 3.4. Variables used in the calculation of the focal distance.

Since the interface is flat, $R_{int} = \infty$, the right part of Equation (6) equals zero., leading to

$$\frac{n_1}{S'} = -\frac{n_2}{S} \tag{7}$$

Rearranging eq. (7), gives that

$$S' = -\frac{n_1}{n_2} S \tag{8}$$

Considering that

$$S = f - h \tag{9}$$

And substituting eq. (2) and (9) into eq. (8), gives that

$$S' = -\frac{n_1}{n_2}\left(\frac{R}{2} - h\right). \tag{10}$$

Therefore, if we want the focus to be on the top surface of the silicon wafer, then

$$S' = t_{Si} \tag{11}$$

where t_{Si} is the thickness of the wafer. Substituting eq. (11) into eq. (10), and the refractive indices, we have that

$$t_{Si} = -2.27\left(\frac{R}{2} - h\right). \tag{12}$$

As aforementioned, the value of t_{Si} is determined by the thickness of the wafer chosen as substrate. Hence, R and h must be calculated to make the right side of eq. (12) equal to that value. For this result, we can consider only the absolute value of the right side, since the sign comes from the optical background of this equation and indicates that this result would be a virtual image.

So, considering the absolute value and substituting eq. (3) into eq. (12), we have

$$t_{Si} = 2.27\left[\frac{1}{2}\left(\frac{h}{2} + \frac{w^2}{8 \times h}\right) - h\right]. \tag{13}$$

Rearranging eq. (1313), gives that

$$12h^2 + \frac{16t_{Si}h}{2.27} - w^2 = 0 \tag{14}$$

Solving it for h, using quadratic equation, and considering only positive results, we have

$$h = \frac{1}{24}\left[-\frac{16}{2.27}t_{Si} + \sqrt{\left(\frac{16}{2.27}t_{Si}\right)^2 - 48w^2}\right]. \tag{15}$$

Substituting eq. (15) into eq. (4), we obtain the initial thickness (t) relative to the hemisphere width (w) and the wafer thickness (t_{Si}). Figure 3.5 shows the ideal t and w for a hemisphere focusing on the top of a wafer with given thickness t_{Si}.

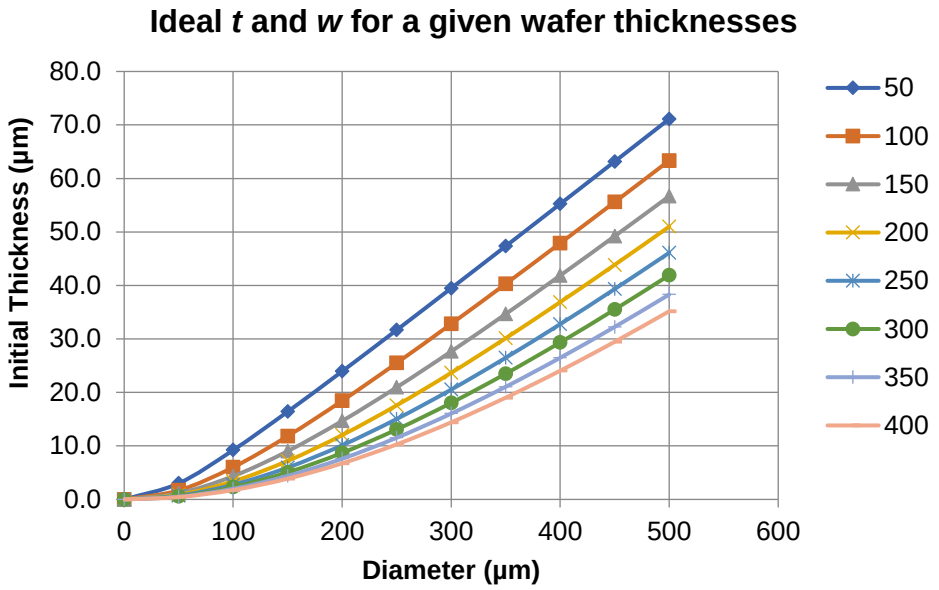

Figure 3.5. Initial thickness and width of hemispheres for given wafer thicknesses.

In case that the focal length f' found is slightly above the interface between the silicon and the top photoresist coating (SC 1827) used in the fabrication, there is no problem. In fact, this is a good thing, because then a spot with a defined area will be illuminated on the top surface, which will facilitate the

fabrication process and the exposure of the photoresist. But since there is another change in the refractive index in this interface, the new normal shift of the focal length must be calculated. For that, eq. (8) becomes

$$S''' = -\frac{n_3}{n_1} S'' \tag{16}$$

where S'' is the distance from the Si/air interface where the focus should be after the shift already caused by the silicon slab; S''' is the distance from the Si/air interface where the focus really is after the new shift due to air (see Figure 3.6); and n_3 is the refractive index of air (=1). Then, the new focal length should be

$$f'' = f' - (S'' - |S'''|). \tag{17}$$

It is important to stress that the shift caused by the top photoresist (SC 1827) is negligible, because the thickness of the photoresist is about 2.5 µm, which is within the error of these calculations.

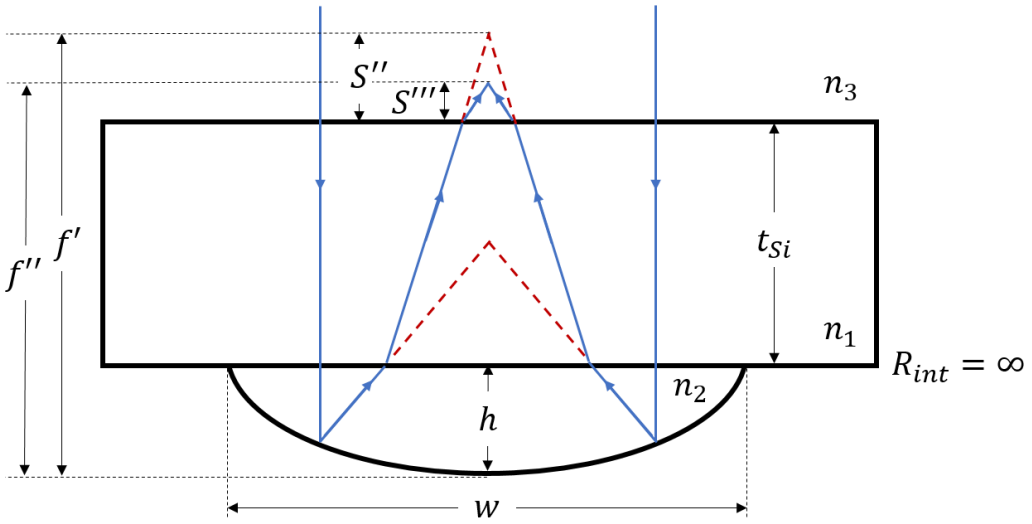

Figure 3.6. Variables describing the calculation of the focal distance with normal shift caused by new interface.

The calculations described allow one to plan and predict the microconcentrator's outline and performance. And the results obtained influenced the fabrication steps taken, which will be explained in Section 4.

3.2. SIMULATION MODELLING

A simulation was done on Zemax OpticStudio to check if the microconcentrator would behave as expected and for comparing the results obtained in the calculations when changing variable parameters. As seen in Figure 3.7, the incoming collinear rays enter the silicon wafer and when they encounter the hemispherical reflective dish at the bottom of the slab, they are reflected back and concentrated on the top surface as planned. The simulation result shows a 150 µm-thick wafer with hemispherical dishes of 230 µm and 250 µm diameters and 40 µm height. These numbers were chosen based on the results of the calculations described in the previous section and the wavelength of light was 980 nm, which is the laser wavelength used in the fabrication process.

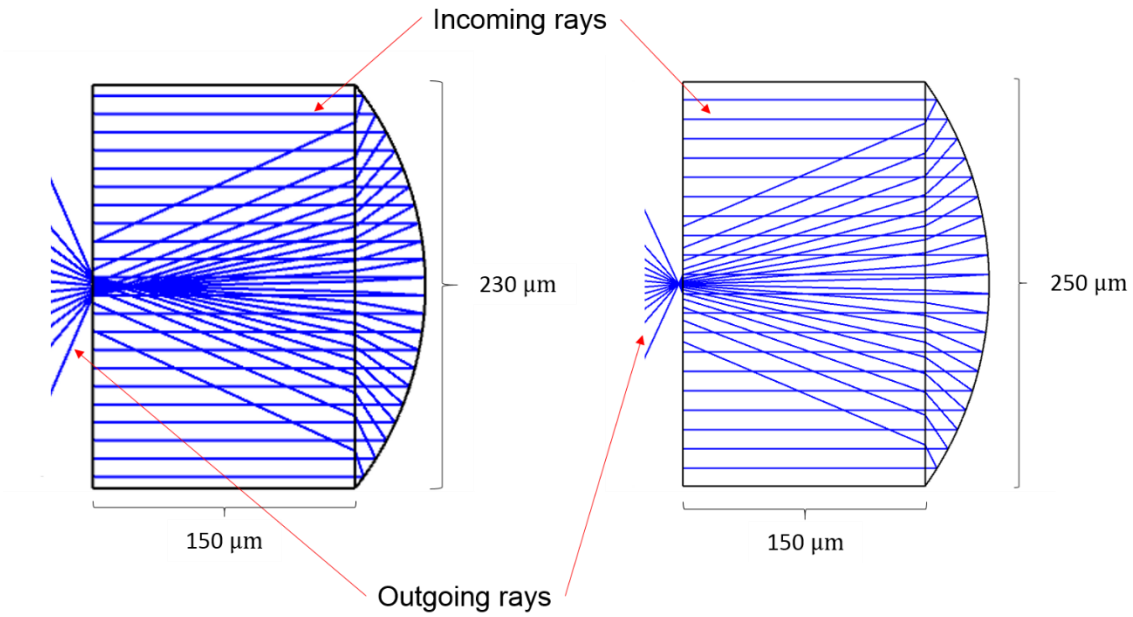

Figure 3.7. Zemax simulation result showing a single microconcentrator of 230 µm (left) and 250 µm (right) diameter and 40 µm height, at the bottom of a 150 µm-thick silicon wafer. Light travels from left to right and is reflected by the microconcentrator back to the top surface (at the left of the slab).

It is possible to observe in this simulation that part of the concentrated rays, the ones that are further away from the centre axis, are not overpassing the top

surface. This leads to the conclusion that they are enclosed in the silicon slab due to total internal reflection. In other words, the deflection caused by the microconcentrators made the angle of incidence of these rays greater than the critical angle, preventing them from passing through the silicon/air interface.

The resulting average focal length in the simulation was similar than that obtained from the calculations.

4. FABRICATION

For fabricating the design mentioned in the previous section, a process flow was developed, which is seen in Figure 4.1. It is composed by two main parts, the first one consists of creating the concave mirrors that will act as microconcentrators; the second involves upconverting photolithography using these microconcentrators to perform an exposure at their focuses.

The processing starts with a double side polished silicon wafer cut into smaller pieces of 2cm x 1.5cm. The substrate is cleaned with acetone, methanol and de-ionized (DI) water, in this order. After dried, it is spin coated with AZ 40XT-11D, which is a positive ultrathick photoresist distributed by MicroChemicals. This photoresist can achieve 15 - 100 µm film thickness, thus, the parameters used during the spin coating step were aiming for a 25 µm result.

After the soft bake, the photoresist is exposed using a direct writer and gets a pattern composed of cylinders after development. These cylinders then go through a reflow step to acquire the hemispherical shape. When cooled down and hardened, the hemispheres are coated with a metal film via sputtering; silver was chosen due to its high reflectivity.

For the second part, a thin positive photoresist Shipley Microposit SC 1827 distributed by MicroChemicals was mixed with upconverting phosphors. More details on the characteristics of these particles are given in Section 4.2.1. The mixture of photoresist and particles was used to spin coat the other surface of the

sample, so an auto-aligned exposure using an infrared laser and the microconcentrators could be done where their focuses are.

Each step of the process flow will be detailed in the next sections. Although the etching step was not pursued due to complications with the previous step and time constraints, it is an important process to create the grooves showed in Figures 3.1 and 3.2. The alignment of these grooves is critical for the solar cell's performance, and that is the reason why an auto-aligned exposure as pursued. Creating these grooves where the microconcentrators' focuses are, will not only increase the surface area of the p-n junction where light is more intense, but it is also critical for guaranteeing light trapping to create total internal reflection in the device.

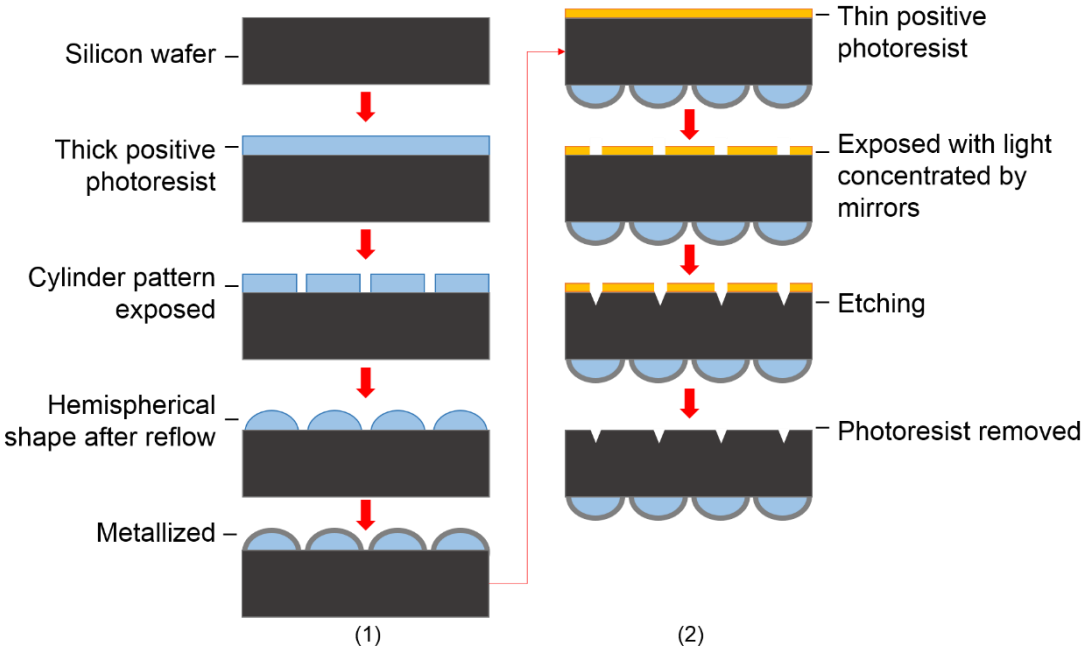

Figure 4.1. Process flow for microconcentrators fabrication.

4.1. MICROCONCENTRATORS

To fabricate the microconcentrators, it was necessary to first make cylinders via photolithography. Then they went through a reflow process to become microlenses. The next step was to coat these hemispherical shapes with a thin

metallic film via sputtering for getting a reflective surface, thus resulting in concave mirrors. More details on the techniques used are given below.

4.1.1. MASKLESS PHOTOLITHOGRAPHY

The cylindrical structures were made using a method of maskless photolithography called direct laser writing. This optical lithography method allows one to transfer micro patterns to photoresist films in a fast, economical, and easy way, without requiring different masks to be created for each design to be tested. It works similarly to a printer, scanning the sample and moving the laser beam to expose the photoresist film according to an electronic design.

The equipment used for the photolithography step was the tabletop Micro Pattern Generator μPG 101 from Heidelberg Instruments, with an ultraviolet diode laser source. An exposure was performed using the design in Figure 4.2, with diameters ranging from 300 μm to 410 μm. The design was created in a bitmap format, using the image editor GNU Image Manipulation Program (GIMP).

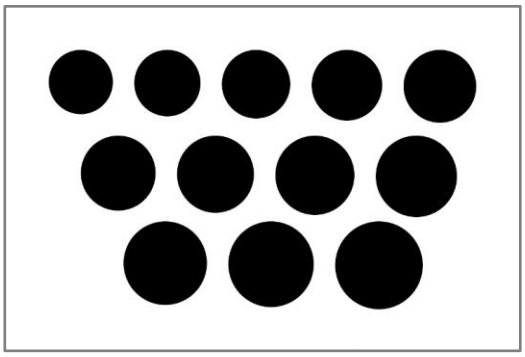

Figure 4.2. Design for exposing the cylinders using the direct writer. Diameters vary from 300 μm (top left) to 410 μm (bottom right) with increments of 10 μm. For a positive resist, the black portion is not exposed, while the white portion is fully exposed.

After exposed, a post exposure bake was done on the sample and then it was developed using AZ 300 MIF Developer distributed by MicroChemicals. Following these steps, the pattern was revealed, with the cylinders raised and the

area surrounding them empty. The result of the maskless photolithography process is shown in Figure 4.3.

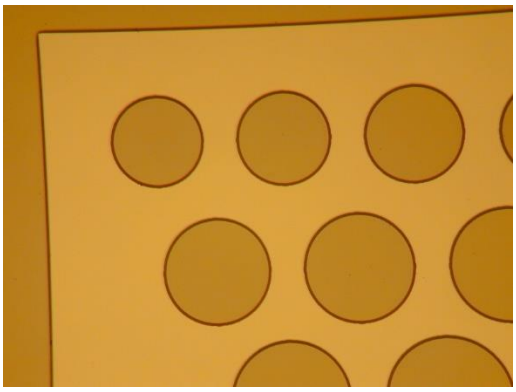

Figure 4.3. Optical microscope image of top left part of sample after direct writing exposure and development.

4.1.2. REFLOW

To transform the cylinders created with direct writing into microlenses, or hemispheres, a reflow step was required. This step was done following the descriptions found in the literature [35]–[37]. Thermal reflow is a method for softening and rounding photoresist structures, often used in the fabrication of microlenses. This transformation is caused by heating the photoresist at a temperature higher than its glass transition temperature, which makes it melt and get the curved shape due to the surface tension effect. To maintain the same volume as before, the final height changes after thermal reflow, but the diameter remains the same. The relation between the initial cylinder and the final lens parameters after reflow is illustrated in Figure 4.4 and expressed by Equation (4), discussed in Section 3.1.

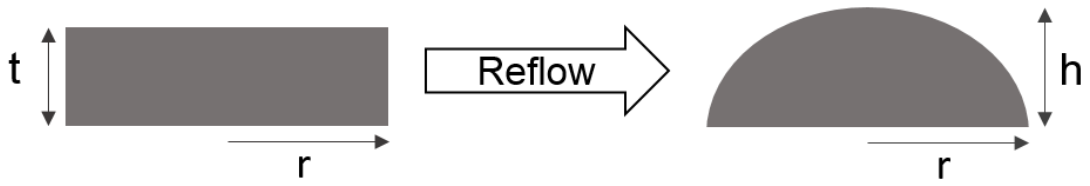

Figure 4.4. Side view of photoresist structures before and after reflow process. The vertical cylinder of thickness *t* becomes the hemisphere of central height *h*. Both have the same half-width *r*.

For example, a cylinder with 27 µm thickness and 380 µm diameter, should result in a hemisphere with height of 52.6 µm after reflow. Figure 4.5 shows the hemispheres created after the reflow step.

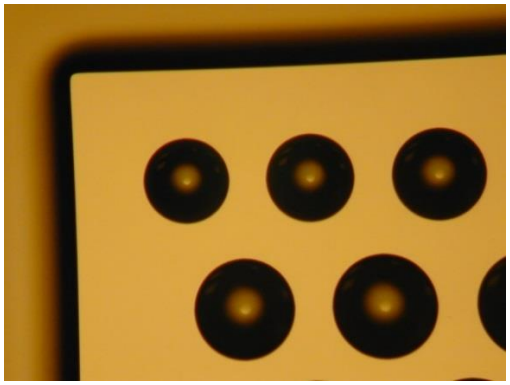

Figure 4.5. Optical microscope image of top left part of sample after reflow.

4.1.3. SPUTTERING

Sputtering is a physical vapour deposition method for coating surfaces with thin films. In this technique, a plasma is created usually with an inert gas as argon, and its particles are accelerated against the target (material which will compose the thin film). When these high energy ions from the gas collide with the target, its atoms are ejected and deposited on the substrate that is on their path, forming the thin film.

To transform the microlenses generated after the reflow step into concave mirrors, a sputtering deposition was done to coat them. The equipment used was Torr International's Compact Research Coater (model number CRC- 600) Sputtering System and the target chosen was silver because of its good reflective properties. Figure 4.6 shows the hemispheres after they were coated with 200 nm of silver.

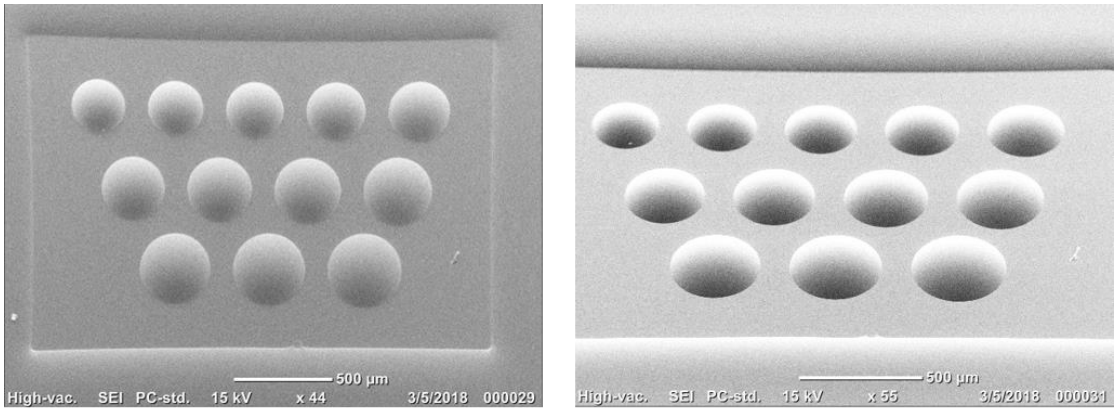

(a) (b)

Figure 4.6. SEM image of sample after metallization. (a) Top view; (b) tilted 45°.

4.1.4. RECIPE

The detailed processing for the microconcentrator's fabrication is summarized in the recipe below:

AZ 40XT-11D Recipe for 25 µm thickness coating

Substrate Cleaning

1. Silicon piece is cleaved into a small piece of 2 cm x 1.5 cm.
2. Rinse sample with acetone for 15 s.
3. Rinse with methanol for 15 s.
4. Rinse with de-ionized (DI) water for 3 min.
5. Blow dry using compressed nitrogen.
6. Dehydrate at 110°C for 2 min.
7. Cool at room temperature (RT) for 5 min.

Spin Coating

8. Dispense photoresist AZ 40XT-11D in a beaker and let it sit for 30 min.
9. Heat photoresist at 65°C on a hot plate for 10 min.

10. Place substrate on spinner and, using a glass syringe, dynamically dispense photoresist on substrate at 100 rpm and wait for 20 s.
11. Spin coat at 3000 rpm for 20 s.

Soft Bake

12. Place sample on hot plate at 65°C on top of a 0.5 cm thick metal support for 1 min.
13. Change the metal support for a 0.25 cm thick one, and ramp the temperature up at a rate of 10°C/30 sec until 125°C.
14. Place the sample directly on hot plate and bake at 125°C for 7 min.
15. Cool at RT for 5 min.

Maskless Photolithography

16. Expose desired design on Direct Writer using write mode III (10 mm) with the parameters: Power at 40% of 70 mW; filter (13%) OFF; overlap x 2; energy mode 1x1; focus 0.

Post Exposure Bake (PEB)

17. Bake sample on hot plate at 105°C for 100 s.
18. Cool down at RT for 5 min.

Development

19. Develop using AZ 300 MIF Developer for 3.5 min.
20. Rinse with DI water for 1 min.
21. Blow dry using compressed nitrogen.

Reflow

22. Place sample on hotplate at 140°C for 60 s.
23. Cool down at RT for 2 min.

Metallization

24. Coat hemispheres with silver (Ag) in the sputtering equipment, based on the parameters:
    - Base pressure: 5.43x10-5 Torr
    - DC gun: 343 V x 0.45 A
    - Gas flow: 10.3sccm
    - Working pressure: 7.2x10-3 Torr
    - Deposition rate: 0.7 Å/s
    - Thickness: 2000 kÅ

4.2. UPCONVERTING PHOTOLITHOGRAPHY

It is a tricky process to get an auto-aligned exposure done where the microconcentrators' focuses are, on the other surface of the substrate. The reason is because light needs to penetrate the silicon slab, hit the concave mirrors in the bottom and get reflected and concentrated at the top of the sample, where the photoresist layer is. Most photoresists used in regular photolithography are exposed with UV light (around 365 nm). But the material used for the proposed solar cell, silicon, strongly absorbs light with wavelengths shorter than its bandgap, which is around 1100 nm. So, a wavelength around 365 nm would be absorbed too fast and not get to the bottom of the slab, then an infrared light source is needed. Figure 4.7 shows a graph with silicon's absorption depending on the wavelength.

A photoresist that could be exposed by light in the near infrared was not available to be purchased. The solution found was to use upconverting particles in a regular photoresist to absorb NIR light and emit UV, exposing the photoresist where the reflected light is focused. Upconverting exposures with similar methods were achieved before in biomaterials applications [39], [40], and they indicated that this technique could be a viable option for us. In the next sections, more explanations on this technique are given.

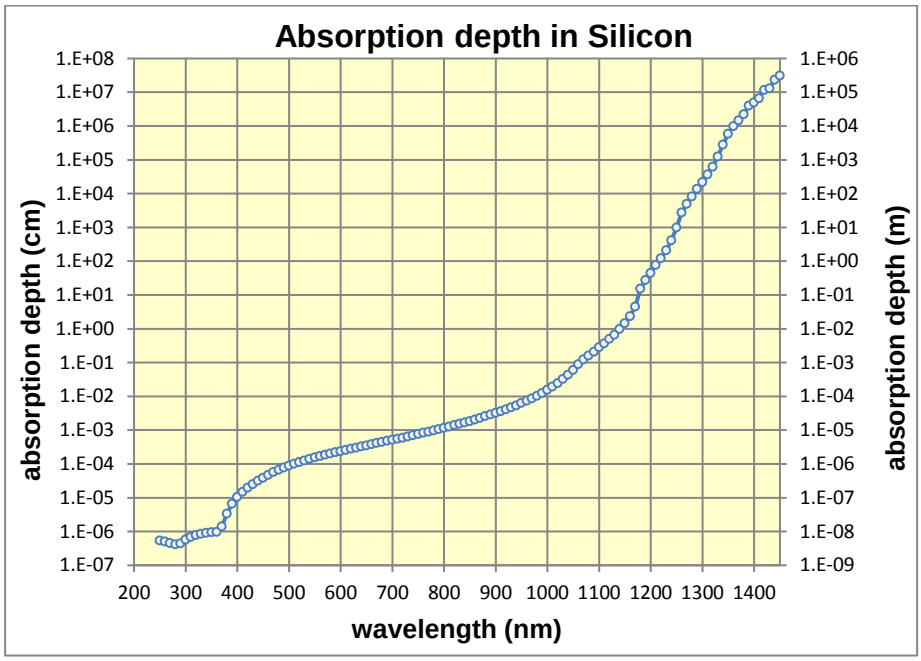

Figure 4.7. Absorption depth in Silicon. Reprinted from [38].

4.2.1. UPCONVERTING PARTICLES

Upconversion happens when long-wavelength radiation (IR or NIR) is transformed into short-wavelength radiation (usually in the visible range). Upconverting particles are excited by absorption of two or more photons and emit light at shorter wavelength than they absorbed. Usually, these particles are phosphors doped with rare-earth materials, and their emission wavelength depends on their dopant. More information on the upconverting particles properties can be found in the references [41].

The upconverting particles used for this study were purchased from Boston Applied Technologies. Their chemical composition is sodium yttrium fluoride: ytterbium, thulium activated ($NaYF_4$:Yb,Tm). Provided as a white powder, the particle size varies from 1 to 4 µm. They are excited by a 980 nm light source and their strongest emission wavelength in the blue light range is at 475 nm. Details on the emission characterization are given in Section 5.2. Phosphors that

are also doped with erbium, present an emission with wavelength around 365 nm, but it is very weak and would not be able to expose the photoresist in the way the experiment was set up to be performed.

The upconverting particles were blended with SC 1827 photoresist and spin coated on the other surface of the silicon wafer (opposite from microconcentrators) to obtain a uniform film of 5 µm thickness. Then the film was exposed using the set-up described in the next section. Figure 4.8 illustrates the upconverting photolithography process.

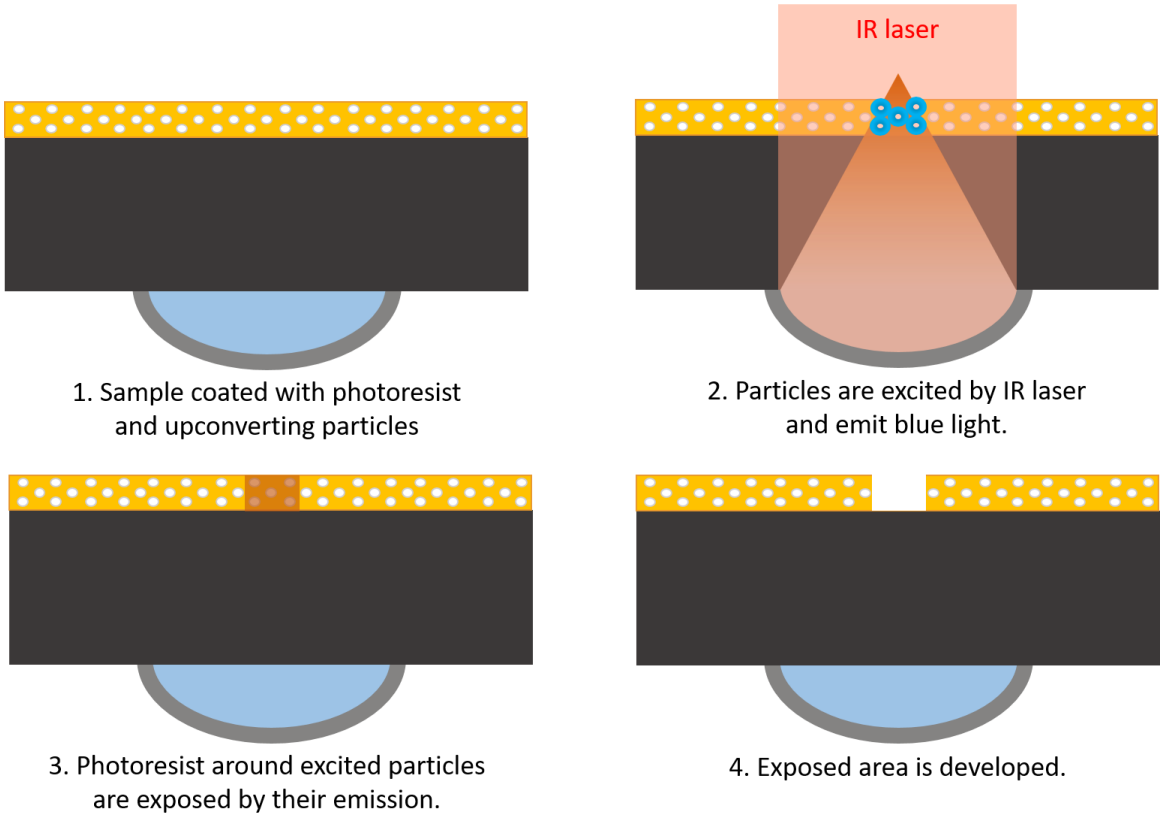

Figure 4.8. Upconverting photolithography process.

4.2.2. Upconverting Photolithography Set-up

To excite the upconverting particles, a 3900S CW Tunable Ti:Sapphire Laser pumped by a 532 nm Millennia eV from Spectra-Physics was used at 975 nm. A polarizer and a half-wave plate were on the laser's path for intensity control. At the wavelength of 975 nm, the absorption depth in silicon is about 97

μm, which means that the light intensity is decreased by a factor of 20 of its original value after transmission through a silicon wafer of 300 μm thickness. But the microconcentrators should enhance the intensity of incoming light by a lot more than 20 times, so the particles can still be excited and expose the photoresist.

To be able to illuminate the whole area occupied by concentrators in the sample, a lens and a beam expander were used on the laser path to focus and expand it without losing power. The sample was placed after the beam expander, as seen in Figure 4.9.

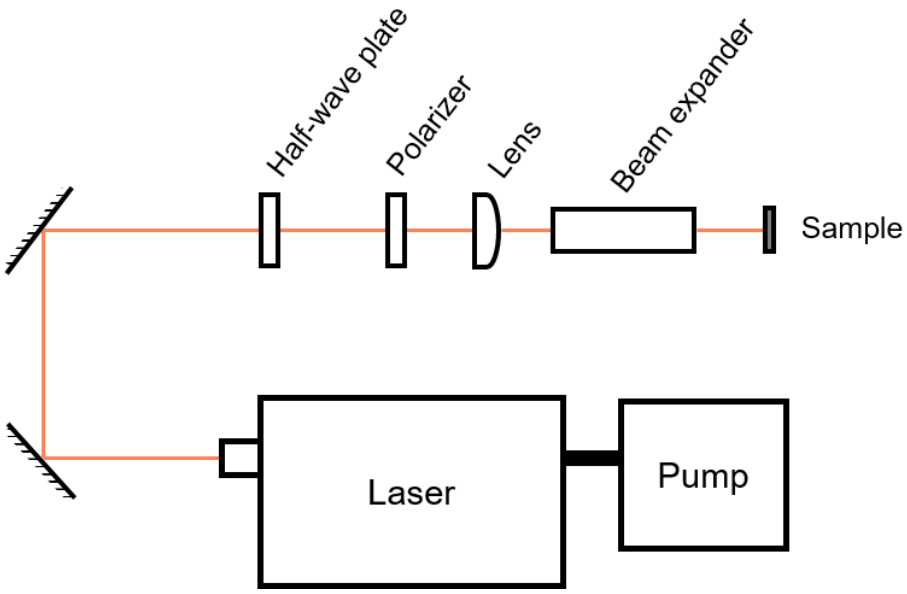

Figure 4.9. Upconverting exposure experimental set up schematic.

4.2.3. RECIPE

The recipe for the upconverting photolithography is detailed below:

SC 1827 + UCP Recipe for 5µm thickness coating

Photoresist Mixture Preparation

1. Pour 4 mL of photoresist SC 1827 in a beaker and add 3200 mg of upconverting particles (UCP).
2. Mix well using a glass rod.
3. Filter with clean wipes that let the particles go through but keep the bubbles and agglomerates away.

Spin Coating

4. Place sample on spinner and using a plastic syringe, dispense photoresist mixture on sample and wait for 30 s.
5. Spin coat at 2000 rpm for 30 s.

Soft Bake

6. Bake sample on hot plate at 110°C for 2 min.
7. Cool at RT for 5 min.

Upconverting Photolithography

8. Expose for the necessary time according to the wafer thickness used.

Development

9. Develop using MF 319 Developer for 45 s.
10. Rinse with DI water for 1 min.
11. Blow dry using compressed nitrogen.

5. CHARACTERIZATION

This section describes characterization methods used for analyzing properties of the microconcentrators, the upconverting particles and the photoresist used in the upconverting exposure.

5.1. MICROCONCENTRATORS PROPERTIES

The microconcentrators were characterized regarding their geometrical and optical properties.

5.1.1. GEOMETRICAL PROPERTIES

As discussed in Chapter 3, geometrical properties such as height and diameter are very important when it comes to predicting the optical properties of the microconcentrators. Therefore, geometrical characterization of the microconcentrators was performed throughout each step of the fabrication. The initial photoresist thickness before and after exposure was measured with Tencor Alpha Step 200 stylus profilometer to ensure it did not change during processing. The height of the hemispherical shapes after reflow was also measured using the profilometer (Figure 5.1). The diameter of the cylindrical shapes before and after turning into and hemisphere was measured using an optical microscope.

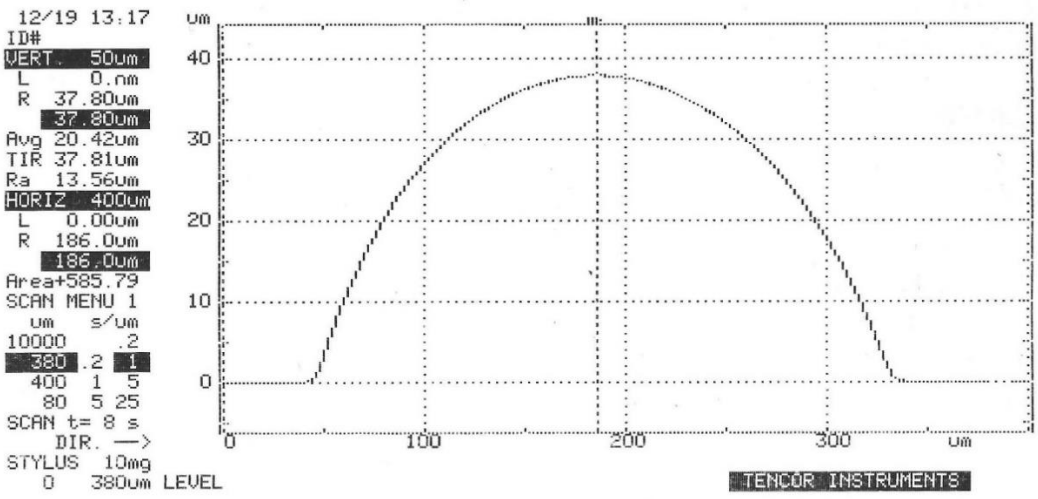

Figure 5.1. Profilometer measurement result showing a concentrator with 280 µm diameter.

5.1.2. Optical Properties

To confirm the ability of the concentrators in focusing incoming light, a setup seen in Figure 5.2 was mounted. It was composed by a white light fiber optic 150 Illuminator from Navitar as the light source, mirrors, a beam splitter, and an Infrared Camera Xenics model XEVA 6259. The standard camera lens was substituted by another one with greater magnification for a better analysis.

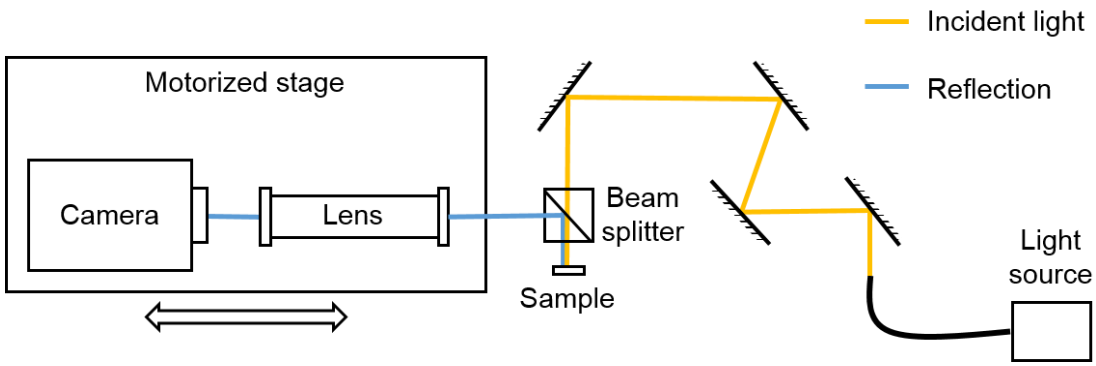

Figure 5.2. Optical characterization set up scheme.

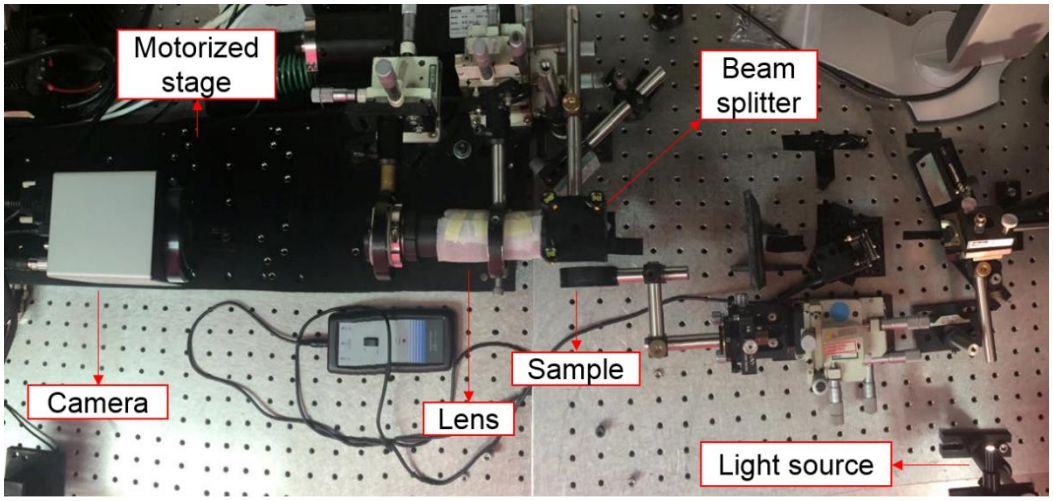

Figure 5.3. Photo of the optical characterization set up.

The sample was placed perpendicular to the incoming light and the beam splitter, so the concentrated light coming from it would be reflected into the camera. The camera and its lens had a fixed distance between them, but they

were placed on top of a motorized stage with controlled step size (ANT180-L Linear Nanopositioner from Aerotech). This arrangement allowed the observation of how the concentrated light spot would change its intensity and size according to the distance between the camera and the sample, with a step size of 10 μm or smaller. This way we could detect where the focal distance was for different configurations of microconcentrators.

Xeneth software (Xenics) allows one to select an area of interest by drawing a line on a spot of the captured image and extract information on the intensity distribution throughout that selection. By placing lines crossing the intense light spots in the centre of the concentrators, it was possible to record the graph provided by this selection tool related to various distances from the sample's top surface (Figure 5.4).

Each concentrator was analyzed, and the graphs associated to each distance observed was saved. The diagrams resulted from this process are Gaussian functions. Therefore, by getting the lowest FWHM (full width at half maximum) from the graphs among one concentrator's set, we could assess at which distance the light spot was stronger, thus determining where the focal distance for that concentrator is.

The method described above works better when the focal distance is located on or above the sample top surface, because it is harder for the camera to capture the light concentrated inside the silicon wafer. This is not a concern since it is of our interest that the light gets more intense right above the silicon surface, so it can excite the particles mixed into the photoresist coating. For this reason, only concentrators focusing above the top surface were characterized.

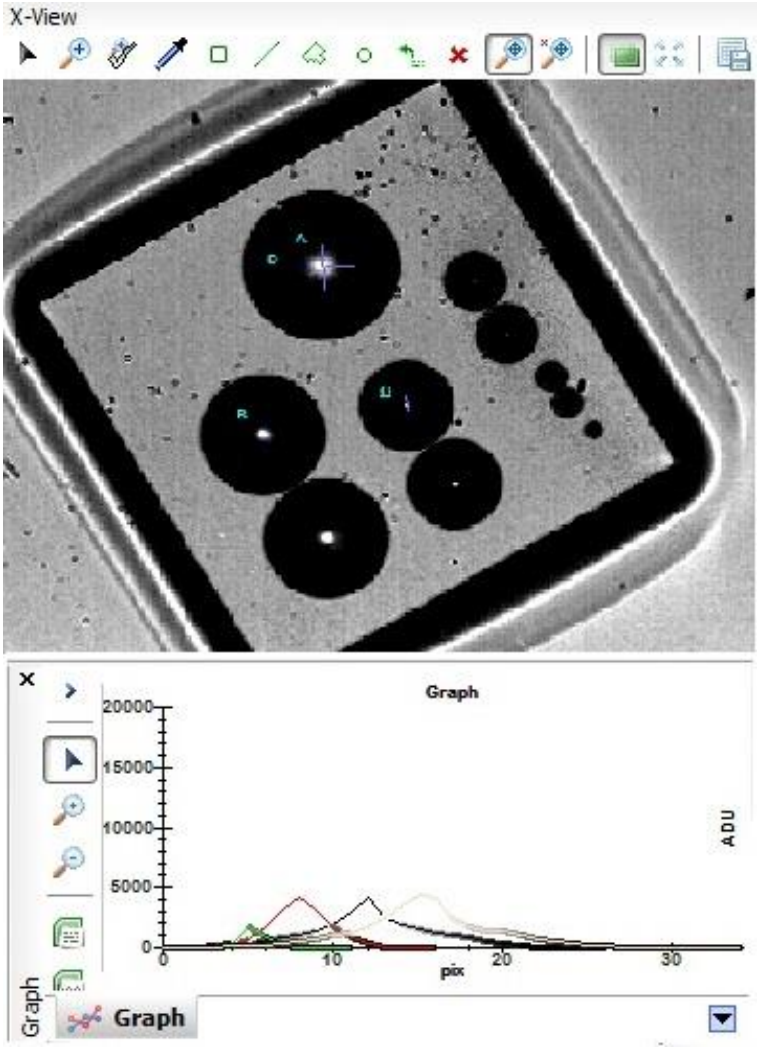

Figure 5.4. Screenshot of the camera software showing selected lines and the intensity graphs generated.

5.2. UPCONVERTING PARTICLES EMISSION

The emission produced by the upconverting particles after excitation was measured by a portable spectroradiometer SR-3501 from Spectral Evolution. The set up for this experiment was similar to the one schematized on Figure 4.8. The sample was composed by 50 mg of UCP powder pressed between two microscope glass slides. And the spectrometer fiber tip was placed right after the sample at an angle, so it would not be saturated by high intensity light coming from the laser and transmitted through the sample.

The result shown in Figure 5.5 was taken using a filter blocking the laser source at wavelengths from 190 to 532 nm, before the beam hit the sample, to ensure no peaks in this range was coming from the light source. It could be observed that when excited by 975 nm, the particles emission has peaks around 480 and 650 nm as it was expected, according to data provided by the manufacturer and in literature records [42], [43].

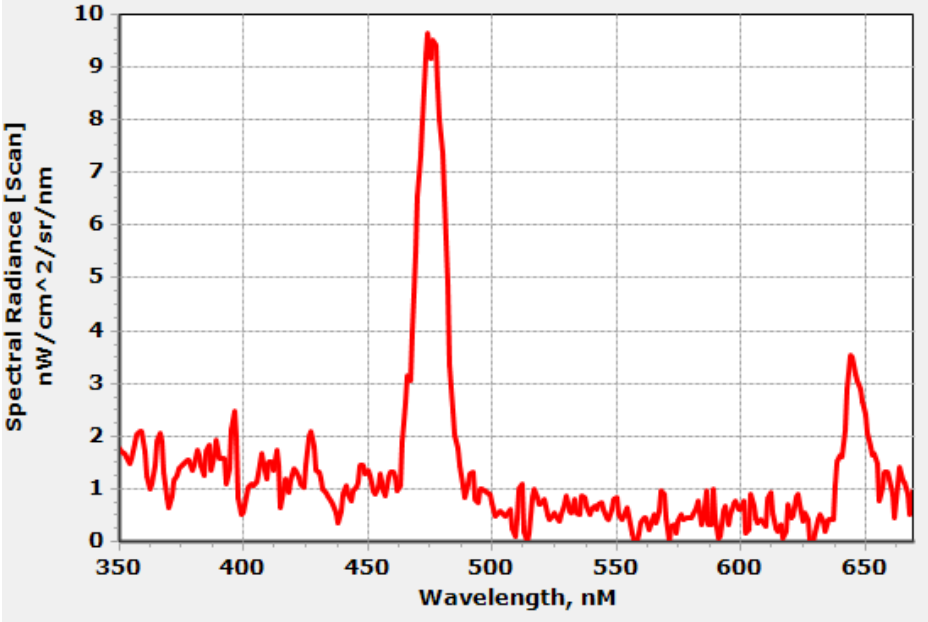

Figure 5.5. Emission spectrum of upconverting particles.

5.3. PHOTORESIST EXPOSURE

According to the manufacturer, SC 1827 photoresist can be exposed by light sources with wavelength ranging from 350 to 450 nm. Therefore, its exposure properties were adjusted for use at 436 nm by the manufacturer. Since the highest emission from the upconverting particles below 650 nm is around 475 nm, it was necessary to confirm if the photoresist could be exposed under radiation of this wavelength.

An absorbance spectrum provided by the manufacturer for the S1800 series (Figure 5.6), which includes SC 1827, shows that the photoresist's absorption

above 440 nm decreases significantly. At 475 nm, it is only a fraction of about 0.1. This means that exposure at this wavelength is still possible, but harder to execute. So, a test was performed to check whether an exposure under this wavelength would work.

For this experiment, a high intensity monochromator from Bausch & Lomb with a tungsten light source was used. It was focused by a lens on a glass slide coated with the photoresist. The size of the projected light spot was 6 mm x 1.5 mm at the focal point of the lens, where the sample was placed.

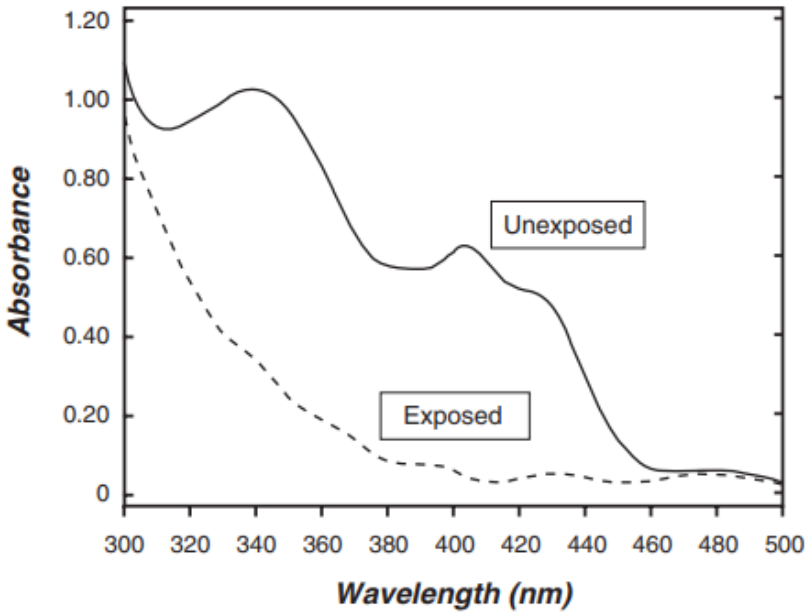

Figure 5.6. Absorbance spectrum of S1800 series photoresist [44].

Spectra resulting from the monochromator's emission measurements showed a broad peak with highest wavelength at 10 nm below the value set on the equipment. This observation can be seen in Figure 5.7 (a). Because of this offset between input and output, the wavelength chosen in the monochromator for the exposure was 10 nm above the desired value, so the output would be where it was supposed to.

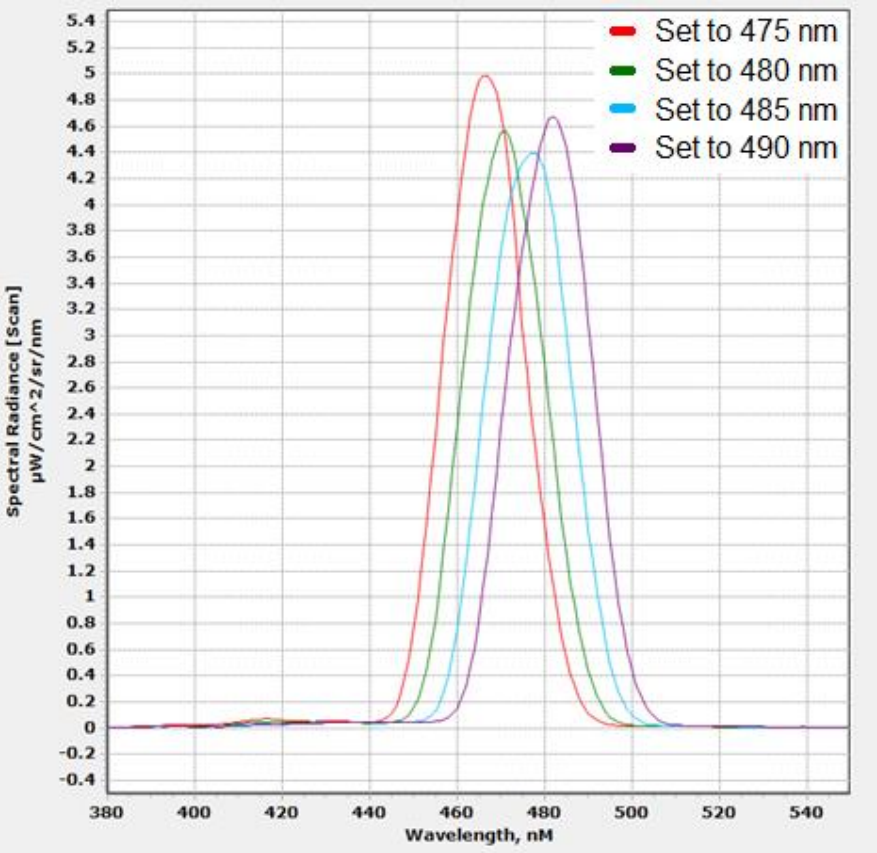

(a)

Selected wavelength (nm)	Output peak (nm)
475	466
480	470
485	477
490	481

(b)

Figure 5.7. Spectral radiance of monochromator output. (a) Spectrometer results showing the output peak wavelength was 10 nm below the selected wavelength in the monochromator. (b) Real peak values.

Two samples were illuminated by the monochromator's focused light. One at a selected wavelength of 475 nm and the other, at 485 nm. In both cases, the photoresist was exposed and cleared after development, as seen in Figure 5.8.

This proved that an exposure under 475 nm was possible and the attempt of doing an upconverting photolithography could work.

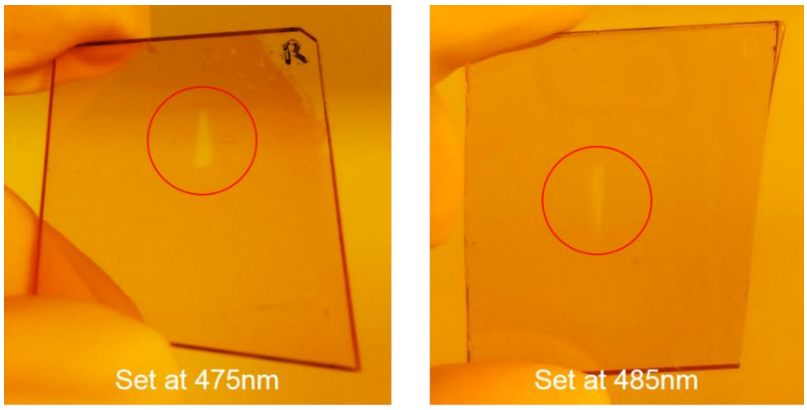

(a) **(b)**

Figure 5.8. Samples exposed by monochromator; (a) set at 475 nm, and (b) set at 485 nm.

5.4. UPCONVERTING EXPOSURE

5.4.1. LASER BEAM PROFILE

The area of the laser beam at its original configuration was smaller than what we needed to perform the upconverting exposure. Therefore, to guarantee that a broader area would be illuminated by the laser, the beam had to be expanded. But to maintain its intensity, the beam was focused before passing through the expander, as described in Section 4.2.2.

In order to assure a consistent set of experiments, the beam was characterized using a Laser Beam Profiler Photon NanoScan 2s Pyro/9/5 from Ophir Photonics. At its best configuration for an upconverting exposure, the laser was set to 975 nm. The output power was around 250 mW as measured using the thermal power meter MAESTRO from Gentec-EO. The area measured by the beam profiler was an ellipse of about 1920 µm by 1650 µm with its intensity following a Gaussian distribution (Figure 5.9).

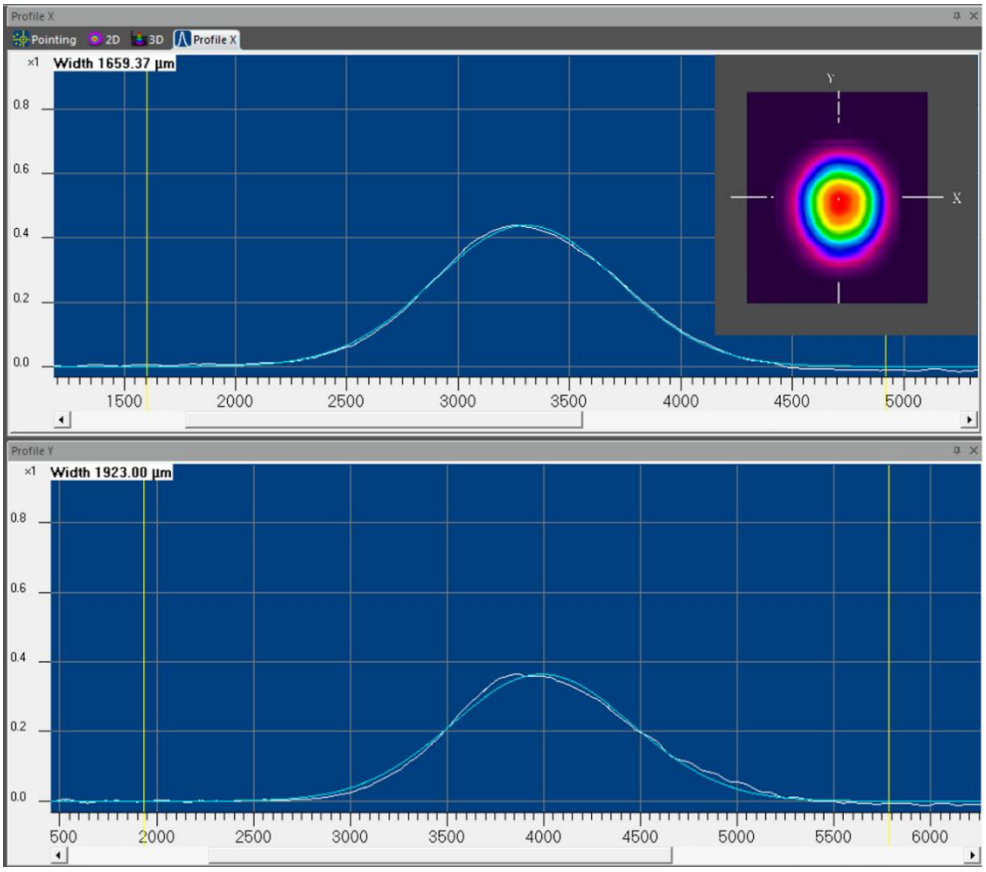

Figure 5.9. Laser beam profile. Top right: 2D profile.

5.4.2. Upconverting Photolithography Using a Mask

To prove that the concept of the upconverting photolithography would work before testing it with the concentrators, an experiment was done using a regular photolithography mask. The pattern was composed by 10 um-thick lines separated by a 100um between them, as seen in Figure 5.10 (b). The mask was placed in front the sample, which was a microscope glass slab coated with photoresist and upconverting particles, prepared as the recipe provided in Section 4.2.3. The laser was focused and expanded, as described in Subsection 5.4.1, and it was illuminating the sample for 2 hours.

The result is shown in Figure 5.10 (c and d). The exposure was successful, however it is noticeable that the resolution is very dependent on the particles size. Even though the stripes are well defined, the edges are not very sharp,

since their thickness is only 2-3 times bigger than the average particle size. It is also important to stress that the exposed area was smaller than the laser beam area hitting the sample. The area exposed in the photoresist was only half the size of the incoming beam, represented by the area inside the green ring on the 2D profile in Figure 5.9.

This experiment proved that the upconverting exposure is possible and it can be a useful tool for anyone who needs to perform photolithography with light sources in the near infrared range.

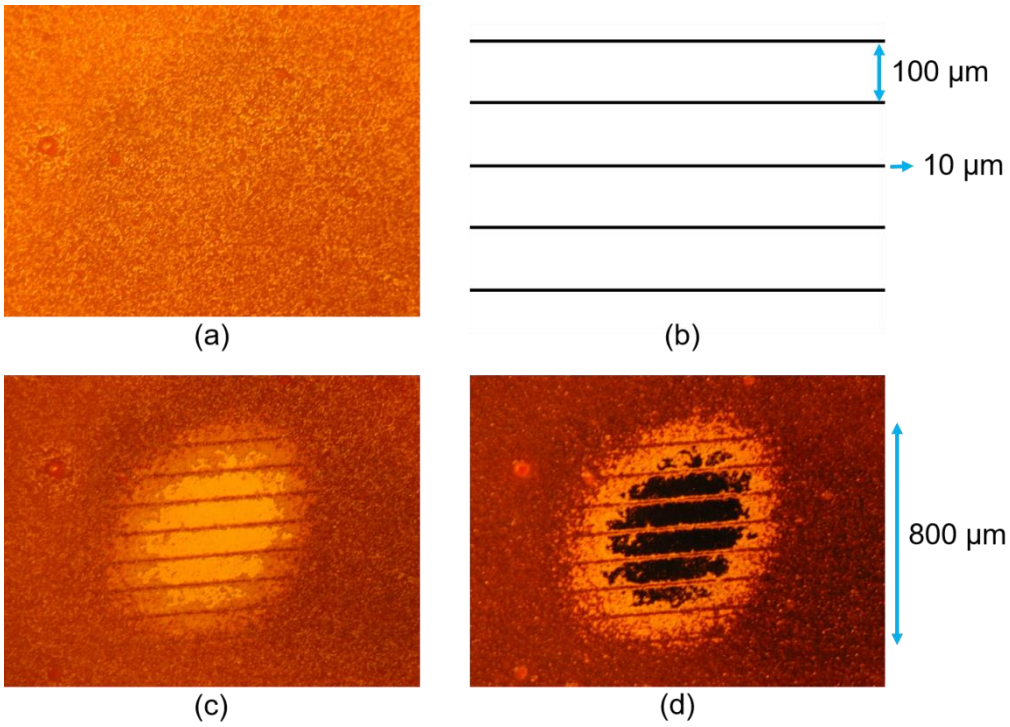

Figure 5.10. Upconverting exposure using a mask. (a) Optical microscope image of the sample before exposure; (b) pattern of the mask; (c) exposed sample on bright field mode; (d) exposed sample on dark field mode.

6. RESULTS

Different microconcentrator diameters were tested throughout the experiments executed during this study and different wafer thicknesses were used. Therefore, results discussed in this section comprise the latest experiments and their outputs.

6.1. GEOMETRICAL PARAMETERS

As stated previously in Section 3.1, the height of the hemispherical shape changes after reflow, and it depends on the shape's diameter and the photoresist's initial thickness. The relation between height and diameter is not linear, so the prediction of the height using the diameter and initial thickness as input it is not straightforward. Considering the initial thickness of the cylinders obtained after the maskless photolithography and measured by contact profilometry, expected heights were calculated using Equation (4) and considering an average thickness (t) of 29 µm. Diameter values varied from 80 to 270 µm. Figure 6.1 shows the heights measured and the theoretical values for the same diameters. It can be said that experimental and theoretical results match, and they agree with results found elsewhere in the literature (Figure 6.2) [45].

The minor differences spotted among smaller diameters can be attributed to non-uniformity of spin coating, causing the initial thickness of the cylinders to vary from 28.7 to 29.7 µm. Even a small variation of t could imply in a different value found as a result from the calculation, especially for smaller radius. The differences could also be caused by difficulty in measuring the final height precisely using the profilometer. Within the available resources, the profilometer was the easiest one to use for this purpose (and reliable enough), but it was difficult to manually determine whether the cantilever tip was passing right on the highest point of the hemisphere's top. For this reason, three or more measurements were done for the same hemisphere and the highest number was

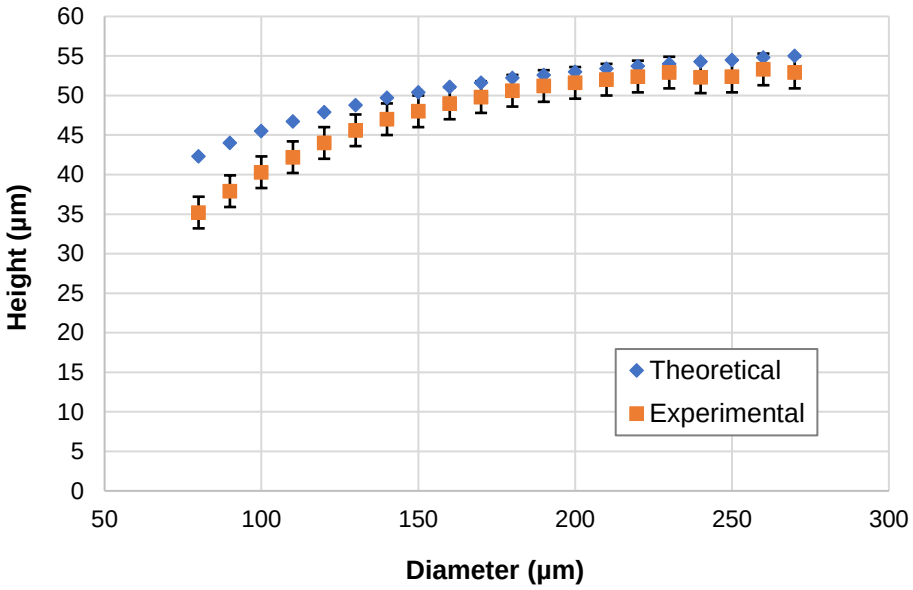

Figure 6.1. Hemisphere height measured at different values of diameter using profilometer, and theoretical values calculated using Equation (4) and average t = 29.0 µm.

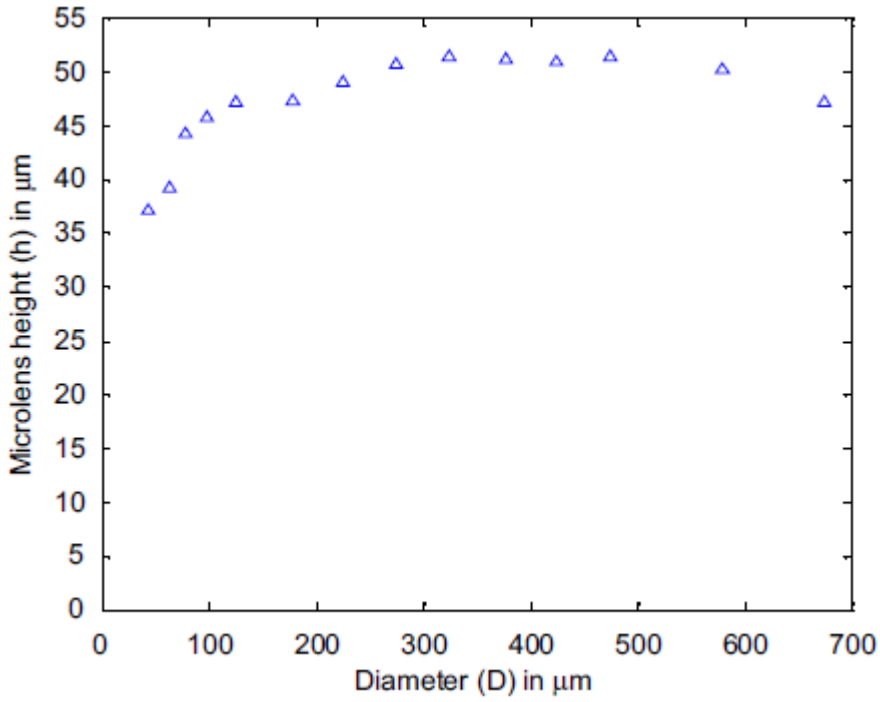

Figure 6.2. Microlens height at different diameters (t = 27.5 µm) from [45].

considered. White light interferometry was another measurement technique tested but it was not suitable for these samples, neither before nor after metallization, because the sample was too transparent or too reflective to be properly recognized by the equipment.

6.2. FOCAL DISTANCE

The experimental set-up described in Section 4.1.2 was very useful to observe the concentration ability of the microconcentrators. Although the motorized stage has very precise steps, the graphs generated by the selection tool would fluctuate too much, making it complicated to obtain quantitative results that could be compared to theoretical data.

Regardless of this inconvenience, it was possible to observe the variation of focal distance among different diameters of the metallized hemispherical shapes. Figure 6.3 shows the varying locations of the focal spots for diameters ranging from 350 to 600 µm, in that order. It is possible to observe that the focal distance of smaller diameters is closer to the top surface of the sample, whereas the focal distances of larger diameters are further, and above the top surface. One can also notice that spherical aberrations are present, and more pronounced with larger diameters.

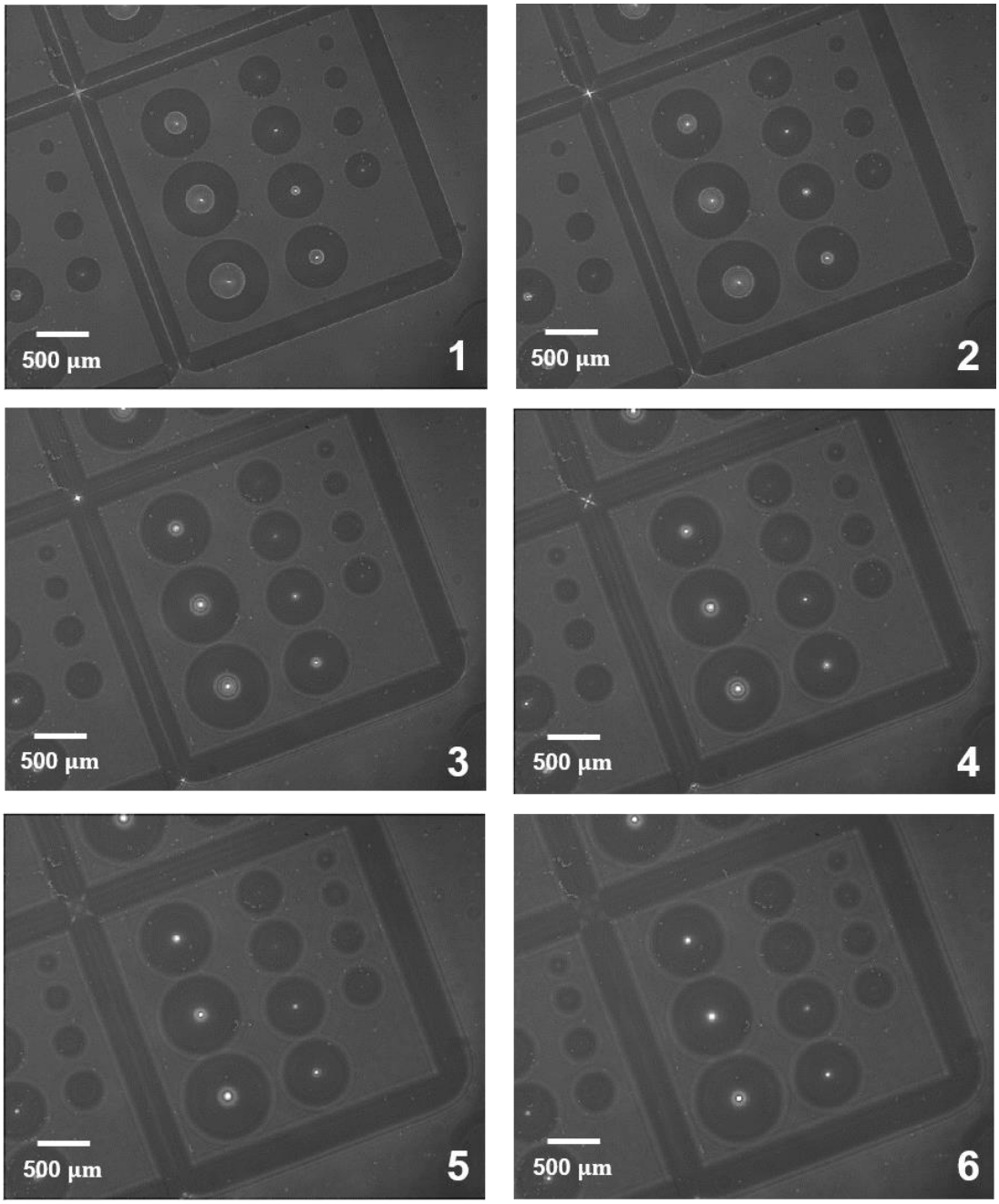

Figure 6.3. Focal distance of microconcentrators with different diameters (350-600 µm). The smaller the diameter, the closer its focus is from the top surface.

6.3. UPCONVERTING EXPOSURE

An auto-aligned upconverting exposure as explained in Section 4.2 was pursued but did not deliver pertinent results. It is believed that the issue might be caused by scattering of incoming light generated by the upconverting particles mixed into the photoresist. This can be leading to a poor concentration of light on the microconcentrator's focus since the rays are not parallel to each other.

Because of that, another strategy using the same set-up described in Figure 4.9 was tested, but the process illustrated in Figure 4.8 changed. The new method of auto-aligned upconverting exposure is performed prior to the metallization of the hemispherical shapes, so they can be used as microlenses, and the direction in which the laser goes through the sample is switched (as illustrated in Figure 6.4). This way, the laser can illuminate the sample from the patterned rear surface and the incident light is focused by the microlenses on the layer of photoresist mixed with upconverting particles at the top surface. With this approach, the upconverting particles do not get in the way of the laser, thus any possible scattering is avoided. Another advantage of this new approach is that the laser absorption in the silicon slab is decreased since the beam passes through the slab only once instead of twice (when it had to go through the slab, hit the microconcentrator and be reflected back to the top surface), which also reduces the time needed for the exposure to happen.

This change in direction of the incoming laser has an effect in the focal length calculation, because now the laser will be refracted two times by the microlens before it gets to the top surface of the silicon slab. The first one will be in the air/photoresist interface, and then again in the photoresist/silicon interface. And according to the calculations presented in Section 3, this makes the focal distance to be longer than when the laser comes from the top surface and is reflected by the metallized microconcentrator. Therefore, to obtain the same focal distance of a microconcentrator, the diameter of the photoresist hemisphere acting as a microlens would have to be smaller.

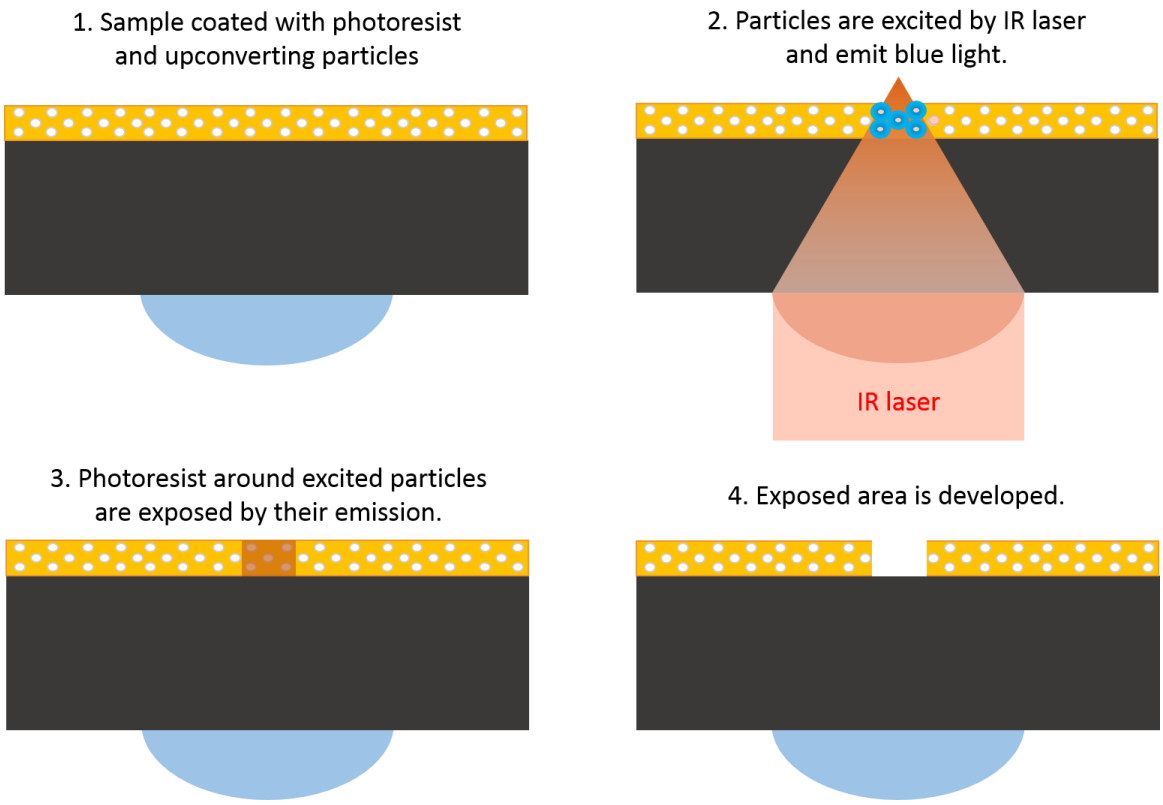

Figure 6.4. Modified upconverting photolithography process.

Even though this new method of auto-aligned upconverting lithography can be easier to perform, no exposure was obtained on the other side of the silicon wafer when following this processing step. The possible reason is that the transmission through the silicon slab was too poor, leaving the laser intensity on the opposite surface to be very weak. Although it was possible to observe the upconverting particles' blue emission, it was not strong enough to expose the photoresist. Therefore, possible solutions to make the auto-aligned upconverting exposure work are: a more powerful laser source and thinner silicon wafers.

7. DISCUSSION

7.1. UPCONVERTING PHOTOLITHOGRAPHY PROCESS

Using upconverting phosphor powdered particles for the upconverting photolithography has the advantage of being practical in the perspective of sample preparation since one just have to incorporate the particles into the photoresist, which allows spin coating to be practiced as usual. However, some constraints were identified. One of them is the resolution of the exposed pattern being determined by the particle size of the powder used, which can be a problem depending on the pattern used and the size of its features. A way to improve uniformity and edge roughness of the exposed spots is to slightly rotate the sample on a stage during the exposure. More details on this strategy can be found in [30]. Another issue caused by the particles is light scattering, which can affect the optical path of the laser, especially in the case of an auto-aligned exposure that needs the laser to pass through the photoresist layer prior to the focused exposure. A possible solution for these concerns might be the use of an upconverting film composed by phosphor nanoparticles instead of micron-sized particles [46].

Since the auto-aligned exposure had to be done using the hemispheres as microlenses before they became microconcentrators (when metallized), it would be ideal for the microlenses and the microconcentrators to have similar focal distances. This could be achieved if the hemisphere was made of silicon instead of photoresist, because this way there would be no refraction in the interface between the microlens/microconcentrator and the silicon slab, since the refractive index would be the same. If the hemisphere was made of silicon, there would still be a difference in focal distance depending on where the light was coming from (top or rear surface) when interacting with the hemisphere. Light would still be refracted in the air/silicon when the hemisphere is acting as a microlens (laser coming from the rear surface), but the difference would be much smaller than if it was made of photoresist. Reactive ion etching (RIE) could be performed to

transfer the hemispherical structure from the photoresist to the silicon wafer. This process was discussed in [37], [47]. Transferring the pattern to silicon is also the next step into build the final solar cell, since it would be a more thermally stable structure, with less chromatic aberrations and it would enable a better electrical contact.

The way the experiments were set up and conducted did not allow one to obtain quantitative measurements of the upconverting efficiency of the phosphor particles, which occasioned in the experiments and the results to be very empirical. This implied in the upconverting photolithography to not have an accurate recipe, especially regarding the exposure time.

7.2. SILICON THICKNESS

A few factors should be considered when choosing the ideal silicon thickness for a solar cell based on the design described in this thesis. The first aspect is light absorption, theoretically an ideal silicon solar cell would be about 100 μm-thick to absorb enough sunlight to deliver a good efficiency. Secondly, thicker silicon wafers are more expensive, which would increase the price of the final product. But thinner wafers are harder to manipulate, especially considering the many steps present in the process flow created to obtain the microconcentrators, which included two spin coatings.

The wafer thickness also affects the hemispheres' parameters since it influences where the focus should be. In addition, thicker wafers increase the upconverting photolithography exposure time, because the laser transmission through the wafer will be significantly reduced. Another aspect to ponder is that when adding the step of reactive ion etching in the process flow, the final thickness of the silicon slab will change due to the etching for the pattern transfer. It is important to keep in mind all these factors when optimizing this design.

7.3. MICROCONCENTRATOR OPTIMIZATION

As observed in the Zemax simulations, the microconcentrators are susceptible to spherical aberration. This effect is observed in real lenses and mirrors, when the light rays strike the optical device near its edges and fail to focus in the same location as the rays that strike the device closer to the its centre. With optimization of the microconcentrator for decreasing spherical aberration, higher concentration of the incoming light can be obtained.

To get a good light trapping in the final solar cell, the microconcentrator array distribution must also be optimized. It is important to find the best ratio between the number of concentrators per area and the area that should be covered by the metal contact on the focus, which will block incoming sunlight to get into the solar cell. Once the best configuration of the microconcentrator array is obtained, another aspect to optimize is the fabrication. It might be possible to lower the cost by using an imprint lithography as replication method, which is an easy and up-scalable process.

8. CONCLUSION

There are different strategies to increase a solar cell's conversion efficiency. Two of them are: light trapping and concentrators. With light trapping, the optical path length of light rays is increased inside the solar cell, which can lead to total internal reflection and better absorption of longer wavelengths by the solar cell. Light trapping is usually achieved by rear surface reflection and texturization of top and rear surfaces. With concentrators, the efficiency is enhanced by increasing the intensity of incoming light that strikes the solar cell. Concentrators can be reflective, refractive and luminescent, with enhancement factors varying from two to thousands of suns.

A new design is proposed in this thesis with the goal of increasing efficiency in silicon solar cells. The concept is to use hemispherical microconcentrators at the rear surface of the solar cell as light trapping structures. Resembling

parabolic dish reflectors, these microconcentrators increase light absorption by focusing incoming light onto a p-n junction placed on top surface of the solar cell, while inducing total internal reflection.

A process flow was presented to fabricate the microconcentrators. The processing included photolithography, thermal reflow and metallization to create the hemispherical microconcentrators. These structures were successfully produced, and it was shown that they were able to concentrate incoming light at their focuses.

A novel type of photolithography was suggested for an auto-aligned exposure of a photoresist film where the microconcentrators' focused are. The so-called upconverting exposure is performed by adding phosphor particles into the photoresist and exciting these particles with an infrared light source to obtain an emission in the visible range, causing the photoresist to be exposed. Although experiments proved this technique works, it was not possible to perform an exposure with the infrared laser passing through a silicon wafer substrate. An alternative way of conducting this experiment was proposed, but no successful result was obtained. It is believed that the laser was too attenuated when transmitted through the silicon slab. Therefore, a more powerful laser source, as well as thinner wafers, are possible solutions to make the auto-aligned upconverting exposure work.

The hemispherical shape's geometry and array disposition requires optimization. The same is true for the upconverting lithography process, that needs further study to prove its effectiveness for the auto-aligned exposure. However, the work presented here shows a promising design and its fabrication method for application in silicon solar cells.

8.1. FUTURE WORK

Besides the optimizations discussed in Section 7, future work should include measuring the light trapping properties of the optimized microconcentrator array.

Subsequent steps would be to create a complete functional solar cell using the design proposed and measure its electrical properties and efficiency. A study on the effect of variation of the angle of incidence in the efficiency could also be conducted.

REFERENCES

[1] REN21, “Renewables 2018 Global Status Report.”, Paris: REN21 Secretariat.

[2] F. Creutzig, P. Agoston, J. C. Goldschmidt, G. Luderer, G. Nemet, and R. C. Pietzcker, “The underestimated potential of solar energy to mitigate climate change,” Nat. Energy, vol. 2, no. 9, p. 17140, 2017.

[3] C. Breyer et al., “On the role of solar photovoltaics in global energy transition scenarios: On the role of solar photovoltaics in global energy transition scenarios,” Prog. Photovolt. Res. Appl., vol. 25, no. 8, pp. 727–745, 2017.

[4] M. B. Prince, “Silicon Solar Energy Converters,” J. Appl. Phys., vol. 26, no. 5, pp. 534–540, 1955.

[5] W. Shockley and H. J. Queisser, “Detailed Balance Limit of Efficiency of p-n Junction Solar Cells,” J. Appl. Phys., vol. 32, no. 3, pp. 510–519, Mar. 1961.

[6] T. TIEDJE, E. YABLONOVITCH, and G. D. CODY, “Limiting Efficiency of Silicon Solar Cells,” p. 6, 1984.

[7] M. J. Kerr, P. Campbell, and A. Cuevas, “Lifetime and efficiency limits of crystalline silicon solar cells,” 2002, pp. 438–441.

[8] A. Richter, M. Hermle, and S. W. Glunz, “Reassessment of the Limiting Efficiency for Crystalline Silicon Solar Cells,” IEEE J. Photovolt., vol. 3, no. 4, pp. 1184–1191, 2013.

[9] R. M. Swanson, “Approaching the 29% limit efficiency of silicon solar cells,” in Conference Record of the Thirty-first IEEE Photovoltaic Specialists Conference, 2005, pp. 889–894.

[10] D. D. Smith, P. Cousins, S. Westerberg, R. D. Jesus-Tabajonda, G. Aniero, and Y.-C. Shen, “Toward the Practical Limits of Silicon Solar Cells,” IEEE J. Photovolt., vol. 4, no. 6, pp. 1465–1469, 2014.

[11] M. A. Green, Y. Hishikawa, E. D. Dunlop, D. H. Levi, J. Hohl-Ebinger, and A. W. Y. Ho-Baillie, “Solar cell efficiency tables (version 52),” Prog. Photovolt. Res. Appl., vol. 26, no. 7, pp. 427–436, 2018.

[12] Kaneka Corporation, “New World Record Established for Conversion Efficiency in a Crystalline Silicon Solar Cell,” 25-Aug-2017. .

[13] E. YABLONOVITCH and G. D. CODY, “Intensity Enhancement in Textured Optical Sheets for Solar Cells,” IEEE Trans. ELECTRON DEVICES, no. 2, p. 6, 1982.

[14] P. Campbell and M. A. Green, “Light trapping properties of pyramidally textured surfaces,” J. Appl. Phys., vol. 62, no. 1, pp. 243–249, Jul. 1987.

[15] J. Gjessing, A. S. Sudbø, and E. S. Marstein, “Comparison of periodic light-trapping structures in thin crystalline silicon solar cells,” J. Appl. Phys., vol. 110, no. 3, p. 033104, 2011.

[16] P. Papet et al., “Pyramidal texturing of silicon solar cell with TMAH chemical anisotropic etching,” Sol. Energy Mater. Sol. Cells, vol. 90, no. 15, pp. 2319–2328, 2006.

[17] H. A. Atwater and A. Polman, “Plasmonics for improved photovoltaic devices,” Nat. Mater., vol. 9, no. 3, pp. 205–213, 2010.

[18] F. Priolo, T. Gregorkiewicz, M. Galli, and T. F. Krauss, “Silicon nanostructures for photonics and photovoltaics,” Nat. Nanotechnol., vol. 9, no. 1, pp. 19–32, 2014.

[19] A. Bozzola, M. Liscidini, and L. C. Andreani, “Photonic light-trapping versus Lambertian limits in thin film silicon solar cells with 1D and 2D periodic patterns,” Opt. Express, vol. 20, no. S2, p. A224, 2012.

[20] M. Peters, J. C. Goldschmidt, T. Kirchartz, and B. Bläsi, “The photonic light trap—Improved light trapping in solar cells by angularly selective filters,” Sol. Energy Mater. Sol. Cells, vol. 93, no. 10, pp. 1721–1727, 2009.

[21] M. A. Green and S. P. Bremner, “Energy conversion approaches and materials for high-efficiency photovoltaics,” Nat. Mater., vol. 16, no. 1, pp. 23–34, 2017.

[22] P. Campbell and M. A. Green, “The limiting efficiency of silicon solar cells under concentrated sunlight,” IEEE Trans. Electron Devices, vol. 33, no. 2, pp. 234–239, 1986.

[23] Y. Wu, P. Eames, T. Mallick, and M. Sabry, “Experimental characterisation of a Fresnel lens photovoltaic concentrating system,” Sol. Energy, vol. 86, no. 1, pp. 430–440, 2012.

[24] D. Chemisana, “Building Integrated Concentrating Photovoltaics: A review,” Renew. Sustain. Energy Rev., vol. 15, no. 1, pp. 603–611, 2011.

[25] L. van Dijk, E. A. P. Marcus, A. J. Oostra, R. E. I. Schropp, and M. Di Vece, “3D-printed concentrator arrays for external light trapping on thin film solar cells,” Sol. Energy Mater. Sol. Cells, vol. 139, pp. 19–26, 2015.

[26] J. P. Morgan, “Light-guide solar panel and method of fabrication thereof,” US 7873257 B2, 18-Jan-2011.

[27] Morgan Solar Inc., “How it works,” Morgan Solar, 07-Aug-2018.

[28] V. E. Ferry et al., “Optimized Spatial Correlations for Broadband Light Trapping Nanopatterns in High Efficiency Ultrathin Film a-Si:H Solar Cells,” Nano Lett., vol. 11, no. 10, pp. 4239–4245, 2011.

[29] A. Zhang et al., “Advanced light-trapping effect of thin-film solar cell with dual photonic crystals,” Nanoscale Res. Lett., vol. 10, no. 1, 2015.

[30] K. Tvingstedt, S. Dal Zilio, O. Inganäs, and M. Tormen, “Trapping light with micro lenses in thin film organic photovoltaic cells,” Opt. Express, vol. 16, no. 26, p. 21608, 2008.

[31] J. H. Karp, E. J. Tremblay, and J. E. Ford, “Planar micro-optic solar concentrator,” Opt. Express, vol. 18, no. 2, p. 1122, Jan. 2010.

[32] J. H. Karp, E. J. Tremblay, J. M. Hallas, and J. E. Ford, “Orthogonal and secondary concentration in planar micro-optic solar collectors,” Opt. Express, vol. 19, no. S4, p. A673, 2011.

[33] A. Peer and R. Biswas, “Nanophotonic Organic Solar Cell Architecture for Advanced Light Trapping with Dual Photonic Crystals,” ACS Photonics, vol. 1, no. 9, pp. 840–847, 2014.

[34] J. K. Tseng, Y. J. Chen, C. T. Pan, T. T. Wu, and M. H. Chung, “Application of optical film with micro-lens array on a solar concentrator,” Sol. Energy, vol. 85, no. 9, pp. 2167–2178, 2011.

[35] F. T. O’Neill and J. T. Sheridan, “Photoresist reflow method of microlens production Part I: Background and experiments,” Opt.-Int. J. Light Electron Opt., vol. 113, no. 9, pp. 391–404, 2002.

[36] H. Yang, C.-K. Chao, M.-K. Wei, and C.-P. Lin, “High fill-factor microlens array mold insert fabrication using a thermal reflow process,” J. Micromechanics Microengineering, vol. 14, no. 8, pp. 1197–1204, 2004.

[37] M. A. Toukhy, M. Puanescu, and S. Meyer, “Improved thermal flow characteristic resist optimized for the manufacturing of microlenses,” 2010, p. 763911.

[38] C. Honsberg and S. Bowden, “PVEducation: Optical Properties of Silicon,” 16-Aug-2018.

[39] A. Stepuk et al., “Use of NIR light and upconversion phosphors in light-curable polymers,” Dent. Mater., vol. 28, no. 3, pp. 304–311, 2012.

[40] Z. Chen, S. He, H.-J. Butt, and S. Wu, “Photon Upconversion Lithography: Patterning of Biomaterials Using Near-Infrared Light,” Adv. Mater., vol. 27, no. 13, pp. 2203–2206, 2015.

[41] M. Haase and H. Schäfer, “Upconverting Nanoparticles,” Angew. Chem. Int. Ed., vol. 50, no. 26, pp. 5808–5829, 2011.

[42] R. H. Page et al., “Upconversion-pumped luminescence efficiency of rare-earth-doped hosts sensitized with trivalent ytterbium,” p. 13, 1998.

[43] H. Zhang, T. Jia, X. Shang, S. Zhang, Z. Sun, and J. Qiu, “Mechanisms of the blue emission of NaYF:Tm3+ nanoparticles excited by an 800 nm continuous wave laser,” Phys. Chem. Chem. Phys., vol. 18, no. 37, pp. 25905–25914, 2016.

[44] MicroChem Corp., “MICROPOSIT S1800® Series Broadband Resists,” 16-Aug-2018.

[45] M. Ashraf, C. Gupta, F. Chollet, S. V. Springham, and R. S. Rawat, “Geometrical characterization techniques for microlens made by thermal reflow of photoresist cylinder,” Opt. Lasers Eng., vol. 46, no. 10, pp. 711–720, 2008.

[46] H. Park et al., “Thin film fabrication of upconversion lanthanide-doped NaYF 4 by a sol-gel method and soft lithographical nanopatterning,” J. Alloys Compd., vol. 728, pp. 927–935, 2017.

[47] M. Eisner, “Transferring resist microlenses into silicon by reactive ion etching,” Opt. Eng., vol. 35, no. 10, p. 2979, Oct. 1996.